

Hydrological variations of the intermediate water masses of the western Mediterranean Sea during the past 20 ka inferred from neodymium isotopic composition in foraminifera and cold-water corals

Quentin Dubois-Dauphin¹, Paolo Montagna^{2,3}, Giuseppe Siani¹, Eric Douville⁴, Claudia Wienberg⁵, Dierk Hebbeln⁵, Zhifei Liu⁶, Nejb Kallel⁷, Arnaud Dapoigny⁴, Marie Revel⁸, Edwige Pons-Branchu⁴, Marco Taviani^{2,9}, Christophe Colin^{1*}

¹Laboratoire Geosciences Paris-Sud (GEOPS), Université de Paris Sud, Université Paris-Saclay, 91405 Orsay, France.

²ISMAR-CNR, via Gobetti 101, 40129 Bologna, Italy.

³Lamont-Doherty Earth Observatory, Columbia University, 61 Route 9W, Palisades, NY 10964, USA

⁴Laboratoire des Sciences du Climat et de l'Environnement, LSCE/IPSL, CEA-CNRS-UVSQ, Université Paris-Saclay, F-91191 Gif-sur-Yvette, France.

⁵MARUM-Center for Marine Environmental Sciences, University of Bremen, Leobener Strasse, 28359 Bremen, Germany.

⁶State Key Laboratory of Marine Geology, Tongji University, Shanghai 200092, China.

⁷Laboratoire Georessources, Matériaux, Environnements et Changements Globaux, LR13ES23, Faculté des Sciences de Sfax, Université de Sfax, BP1171, 3000 Sfax, Tunisia.

⁸Geoazur, UNS, IRD, OCA, CNRS, 250 rue Albert Einstein, 06500 Valbonne, France

⁹Biology Department, Woods Hole Oceanographic Institution, 266 Woods Hole Road, Woods Hole, MA 02543, USA.

Correspondence to: Christophe Colin (christophe.colin@u-psud.fr)

Abstract. We present the neodymium isotopic composition (ϵNd) of mixed planktonic foraminifera species from a sediment core collected at 622 m water depth in the Balearic Sea, as well as ϵNd of scleractinian cold-water corals (CWC; *Madrepora oculata*, *Lophelia pertusa*) retrieved in the Alboran Sea (280-414 m water depth) and the south Sardinian continental margin (414 m water depth). The aim is to constrain hydrological variations at intermediate depths in the western Mediterranean Sea during the last 20 kyr. Planktonic (*Globigerina bulloides*) and benthic (*Cibicidoides pachyderma*) foraminifera from the Balearic Sea were also analyzed for stable oxygen ($\delta^{18}\text{O}$) and carbon ($\delta^{13}\text{C}$) isotopes. The foraminiferal and coral ϵNd values from the Balearic and Alboran Sea are comparable over the last ~13 kyr, with mean values of -8.94 ± 0.26 (1σ ; $n=24$) and -8.91 ± 0.18 (1σ ; $n=25$), respectively. Before 13 ka BP, the foraminiferal ϵNd values are slightly lower (-9.28 ± 0.15) and tend to reflect higher mixing between intermediate and deep waters, which are characterized by more unradiogenic ϵNd values. The slight ϵNd increase after 13 ka BP is associated to a decoupling in the benthic foraminiferal $\delta^{13}\text{C}$ composition between intermediate and deeper depths, which started at ~16 ka BP. This suggests an earlier stratification of the water masses and a subsequent reduced contribution of unradiogenic ϵNd from deep waters. The CWC from the Sardinia Channel show a much larger scatter of ϵNd values, from -8.66 ± 0.30 to -5.99 ± 0.50 , and a lower average (-7.31 ± 0.73 ; $n=19$) compared to the CWC and foraminifera from the Alboran and Balearic Sea, indicative of intermediate waters sourced from the Levantine basin. At the time of sapropel S1 deposition (10.2 to 6.4 ka), the ϵNd values of the Sardinian CWC become more unradiogenic (-8.38 ± 0.47 ; $n=3$ at ~8.7 ka BP), suggesting a significant contribution of intermediate waters originated from the western basin. We propose

47 that western Mediterranean intermediate waters replaced the Levantine Intermediate Water (LIW), which would
48 be strongly reduced during the mid-sapropel (~8.7 ka BP). This observation supports a notable change of
49 Mediterranean circulation pattern centered on sapropel S1 that needs further investigations to be confirmed.

50

51 **1. Introduction**

52 The Mediterranean Sea is a mid-latitude semi-enclosed basin, characterized by evaporation exceeding
53 precipitation and river runoff, where the inflow of fresh and relatively warm surface Atlantic water is
54 transformed into saltier and cooler (i.e. denser) intermediate and deep waters. Several studies have demonstrated
55 that the Mediterranean thermohaline circulation was highly sensitive to both the rapid climatic changes
56 propagated into the basin from high latitudes of the Northern Hemisphere (Cacho et al., 1999, 2000, 2002;
57 Moreno et al., 2002, 2005; Paterne et al., 1999; Martrat et al., 2004; Sierro et al., 2005; Frigola et al., 2007,
58 2008) and orbitally-forced modifications of the eastern Mediterranean freshwater budget mainly driven by
59 monsoonal river runoff from the subtropics (Rohling et al., 2002; 2004; Bahr et al., 2015). A link between the
60 intensification of the Mediterranean Outflow Water (MOW) and the intensity of the Atlantic Meridional
61 Overturning Circulation (AMOC) was proposed (Cacho et al., 1999, 2000, 2001; Bigg and Wadley, 2001; Sierro
62 et al., 2005; Voelker et al., 2006) and recently supported by new geochemical data in sediments of the Gulf of
63 Cádiz (Bahr et al., 2015). In particular, it has been suggested that the intensity of the MOW and, more generally,
64 the variations of the thermohaline circulation of the Mediterranean Sea could play a significant role in triggering
65 a switch from a weakened to an enhanced state of the AMOC through the injection of saline Mediterranean
66 waters in the intermediate North Atlantic at times of weak AMOC (Rogerson et al., 2006; Voelker et al., 2006;
67 Khélifi et al., 2009). The Mediterranean intermediate waters, notably the Levantine Intermediate Water (LIW),
68 which represent today up to 80 % in volume of the MOW (Kinder and Parilla, 1987) are considered an important
69 driver of MOW-derived salt into the North Atlantic. Furthermore, the LIW also plays a key role in controlling
70 the deep-sea ventilation of the Mediterranean basin, being strongly involved in the formation of deep waters in
71 the Aegean Sea, Adriatic Sea, Tyrrhenian Sea and Gulf of Lions (Millot and Taupier-Letage, 2005). It is
72 hypothesized that a reduction of intermediate and deep-water formation as a consequence of surface hydrological
73 changes in the eastern Mediterranean basin acted as a precondition for the sapropel S1 deposition by limiting the
74 oxygen supply to the bottom waters (De Lange et al., 2008; Rohling et al., 2015; Tachikawa et al., 2015).
75 Therefore, it is crucial to gain a more complete understanding of the variability of the Mediterranean
76 intermediate circulation in the past and its impact on the MOW outflow and, in general, on the Mediterranean
77 thermohaline circulation.

78 Previous studies have mainly focused on the glacial variability of the deep-water circulation in the western
79 Mediterranean basin (Cacho et al., 2000, 2006; Sierro et al., 2005; Frigola et al., 2007, 2008). During the Last
80 Glacial Maximum (LGM), strong deep-water convection took place in the Gulf of Lions, producing cold, well-
81 ventilated western Mediterranean Deep Water (WMDW) (Cacho et al., 2000, 2006; Sierro et al., 2005), while
82 the MOW flowed at greater depth in the Gulf of Cádiz (Rogerson et al., 2005; Schönfeld and Zahn, 2000). With
83 the onset of the Termination 1 (T1) at about 15 ka, the WMDW production declined until the onset of the
84 Holocene due to the rising sea level, with a relatively weak mode during the Heinrich Stadial 1 (HS1) and the
85 Younger Dryas (YD) (Sierro et al., 2005; Frigola et al., 2008), that led to the deposition of the Organic Rich
86 Layer 1 (ORL1; 14.5-8.2 ka BP; Cacho et al., 2002).

87 Because of the disappearance during the Early Holocene of specific epibenthic foraminiferal species, such as
88 *Cibicoides* spp., which are commonly used for paleohydrological reconstructions, information about the
89 Holocene variability of the deep-water circulation in the western Mediterranean are relatively scarce and are
90 mainly based on grain size analysis and sediment geochemistry (e.g. Frigola et al., 2007). These authors have
91 identified four distinct phases representing different deep-water overturning conditions in the western
92 Mediterranean basin during the Holocene, as well as centennial- to millennial-scale abrupt events of overturning
93 reinforcement.

94 Faunal and stable isotope records from benthic foraminifera located at intermediate depths in the eastern basin
95 reveal well-ventilated LIW during the last glacial period and deglaciation (Kuhnt et al., 2008; Schmiedl et al.,
96 2010). Similarly, a grain-size record obtained from a sediment core collected within the LIW depth range (~500
97 m water depth) at the east Corsica margin also documents enhanced bottom currents during the glacial period
98 and for specific time intervals of the deglaciation, such as HS1 and YD (Toucanne et al., 2012). The Early
99 Holocene is characterized by a collapse of the LIW (Kuhnt et al., 2008; Schmiedl et al., 2010; Toucanne et al.,
100 2012) synchronous with the sapropel S1 deposition (10.2 – 6.4 cal ka BP; Mercone et al., 2000). Proxies for
101 deep-water conditions reveal the occurrence of episodes of deep-water overturning reinforcement in the eastern
102 Mediterranean basin at 8.2 ka BP (Rohling et al., 1997, 2015; Kuhnt et al., 2007; Abu-Zied et al., 2008, Siani et
103 al., 2013; Tachikawa et al., 2015), responsible for the interruption of the sapropel S1 in the eastern Mediterranean
104 basin (Mercone et al., 2001; Rohling et al., 2015).

105 Additional insights into Mediterranean circulation changes may be gained using radiogenic isotopes, such as
106 neodymium, that represent reliable tracers for constraining water-mass mixing and sources (Goldstein and
107 Hemming, 2003, and references therein). It has recently been shown that the neodymium (Nd) isotopic
108 composition, expressed as $\epsilon\text{Nd} = \left(\frac{(^{143}\text{Nd}/^{144}\text{Nd})_{\text{sample}}}{(^{143}\text{Nd}/^{144}\text{Nd})_{\text{CHUR}}} - 1 \right) \times 10000$ (CHUR: Chondritic
109 Uniform Reservoir [Jacobsen and Wasserburg, 1980]) of living and fossil scleractinian CWC faithfully traces
110 intermediate and deep-water mass provenance and mixing of the ocean (e.g. van de Flierdt et al., 2010; Colin et
111 al., 2010; López Correa et al., 2012; Monterro-Serrano et al., 2011, 2013; Copard et al., 2012). Differently from
112 the CWC, the ϵNd composition of fossil planktonic foraminifera is not related to the ambient seawater at
113 calcification depth but reflects the bottom and/or pore water ϵNd , due to the presence of authigenic Fe-Mn
114 coatings precipitated on their carbonate shell after deposition onto the sediment (Roberts et al., 2010; Elmore et
115 al., 2011; Piotrowski et al., 2012; Tachikawa et al., 2014; Wu et al., 2015). Therefore, the ϵNd composition of
116 planktonic foraminiferal tests can be used as a useful tracer of deep-water circulation changes in the past,
117 although the effect of pore water on foraminiferal ϵNd values could potentially complicate the interpretation
118 (Tachikawa et al., 2014).

119 In the Mediterranean Sea, modern seawater ϵNd values display a large range from ~-11 to ~-5, and a clear
120 vertical and longitudinal gradient, with more radiogenic values encountered in the eastern basin and typically at
121 intermediate and deeper depths (Spivack and Wasserburg 1988; Henry et al., 1994; Tachikawa et al., 2004;
122 Vance et al., 2004). Considering this large ϵNd contrast, ϵNd recorded in fossil CWC and planktonic
123 foraminifera from the Mediterranean offers great potential to trace intermediate and deep-water mass exchange
124 between the two basins, especially during periods devoid of key epibenthic foraminifera, such as the sapropel S1
125 or ORL1 events.

126 Here, the ϵNd of planktonic foraminifera from a sediment core collected in the Balearic Sea and CWC samples

127 from the Alboran Sea and the Sardinia Channel was investigated to establish past changes of the seawater ϵNd at
128 intermediate depths and constrain hydrological variations of the LIW during the last ~20 kyr. The ϵNd values
129 have been combined with stable oxygen ($\delta^{18}\text{O}$) and carbon ($\delta^{13}\text{C}$) isotope measurements of benthic (*Cibicidoides*
130 *pachyderma*) and planktonic (*Globigerina bulloides*) foraminifera and sea-surface temperature estimates by
131 modern analogue technique (MAT). Results reveal significant ϵNd variations at intermediate depths in the
132 western basin interpreted as a drastic reduction of the hydrological exchanges between the western and eastern
133 Mediterranean Sea and the subsequent higher proportion of intermediate water produced in the Gulf of Lions
134 during the time interval corresponding to the sapropel S1 deposition.

135
136

137 2. Seawater ϵNd distribution in the Mediterranean Sea

138 The Atlantic Water (AW) enters the Mediterranean Sea as surface inflow through the Strait of Gibraltar with an
139 unradiogenic ϵNd signature of ~-9.7 in the strait (Tachikawa et al., 2004) and ~-10.4 in the Alboran Sea
140 (Tachikawa et al., 2004, Spivack and Wasserburg, 1988) for depths shallower than 50 m. During its eastward
141 flowing, AW mixes with upwelled Mediterranean Intermediate Water forming the Modified Atlantic Water
142 (MAW) that spreads within the basin (Millot and Taupier-Letage, 2005) (Fig.1). The surface water ϵNd values
143 (shallower than 50 m) range from -9.8 to -8.8 in the western Mediterranean basin (Henry et al., 1994; Montagna,
144 pers. comm., 2016) and -9.3 to -4.2 in the eastern basin, with seawater off the Nile delta showing the most
145 radiogenic values (Tachikawa et al., 2004; Vance et al., 2004; Montagna, pers. comm., 2016). The surface waters
146 in the eastern Mediterranean basin become denser due to strong mixing and evaporation caused by cold and dry
147 air masses flowing over the Cyprus-Rhodes area in winter, and eventually sink leading to the formation of LIW
148 (Ovchinnikov, 1984; Lascaratos et al., 1993, 1998; Malanotte-Rizzoli et al., 1999; Pinardi and Masetti, 2000).
149 The LIW spreads throughout the entire Mediterranean basin at depths between ~150-200 m and ~600-700 m,
150 and is characterized by more radiogenic ϵNd values ranging from -7.9 to -4.8 (average value $\pm 1\sigma$: -6.6 ± 1) in
151 the eastern basin and from -10.4 to -7.58 (-8.7 ± 0.9) in the western basin (Henry et al., 1994; Tachikawa et al.,
152 2004; Vance et al., 2004; Montagna, pers. comm., 2016). The LIW acquires its ϵNd signature mainly from the
153 partial dissolution of Nile River particles (Tachikawa et al., 2004), which have an average isotopic composition
154 of -3.25 (Weldeab et al., 2002), and the mixing along its path with overlying and underlying water masses with
155 different ϵNd signatures. The LIW finally enters the Atlantic Ocean at intermediate depths through the Strait of
156 Gibraltar with an average ϵNd value of -9.2 ± 0.2 (Tachikawa et al., 2004; Montagna, pers. comm., 2016).

157 The WMDW is formed in the Gulf of Lions due to winter cooling and evaporation followed by mixing between
158 surface waters and the more saline LIW and spreads into the Balearic basin and Tyrrhenian Sea between ~2000
159 m and 3000 m (Millot, 1999; Schroeder et al., 2013) (Fig. 1). The WMDW is characterized by an average ϵNd
160 value of -9.4 ± 0.9 (Henry et al., 1994; Tachikawa et al., 2004; Montagna, pers. comm., 2016). Between the
161 WMDW and the LIW (from ~700 to 2000 m), the Tyrrhenian Deep Water (TDW) has been found (Millot et al.,
162 2006), which is produced by the mixing between WMDW and Eastern Mediterranean Deep Water (EMDW) that
163 cascades in the Tyrrhenian Sea after entering through the Strait of Sicily (Millot, 1999, 2009; Astraldi et al.,
164 2001). The TDW has an average ϵNd value of -8.1 ± 0.5 (Montagna, pers. comm., 2016).

165
166

3. Material and methods

167 3.1. Cold-water coral and foraminifera samples

168 Forty-four CWC samples belonging to the species *Lophelia pertusa* and *Madrepora oculata* collected from the
169 Alboran Sea and the Sardinia Channel were selected for this study (Fig. 1). Nineteen fragments were collected at
170 various core depths from a coral-bearing sediment core (RECORD 23; 38°42.18' N; 08°54.75' E; Fig. 1)
171 retrieved from 414 m water depth in the "Sardinian Cold-Water Coral Province" (Taviani et al., 2015) during the
172 R/V Urania cruise "RECORD" in 2013. The core contains well-preserved fragments of *M. oculata* and *L.*
173 *pertusa* embedded in a brownish muddy to silty carbonate-rich sediment. The Sardinian CWC samples were
174 used for U-series dating and Nd isotopic composition measurements. For the southern Alboran Sea, twenty-five
175 CWC samples were collected at water depths between 280 and 442 m in the "eastern Melilla Coral Province"
176 (Fig. 1) during the R/V Poseidon cruise "POS-385" in 2009 (Hebbeln et al., 2009). Eleven samples were
177 collected at the surface of two coral mounds (New Mound and Horse Mound) and three coral ridges (Brittlestar
178 ridges I, II and III), using a box corer and a remotely operated vehicle (ROV). In addition, fourteen CWC
179 samples were collected from various core depths of three coral-bearing sediment cores (GeoB13728, 13729 and
180 13730) retrieved from the Brittlestar ridge I. Details on the location of surface samples and cores collected in the
181 southern Alboran Sea and details on the radiocarbon ages obtained from these coral samples are reported in Fink
182 et al. (2013). Like the CWC sample set from the Sardinia Channel, the dated Alboran CWC samples were also
183 used for further Nd isotopic composition analyses in this study.

184 In addition, a deep-sea sediment core (barren of any CWC fragments) was recovered southwest of the Balearic
185 Sea at 622 m water depth during the R/V Le Suroît cruise "PALEOCINAT II" in 1992 (SU92-33; 35°25.38' N;
186 0°33.86' E; Fig. 1). The core unit, which consists of 2.1 m of grey to brown carbonaceous clays, was sub-
187 sampled continuously at 5-10 cm intervals for a total number of 24 samples used for $\delta^{18}\text{O}$, $\delta^{13}\text{C}$ and ϵNd
188 analyzes.

190 3.2. Analytical procedures on cold-water coral samples

191 3.2.1. U/Th dating

192 The nineteen CWC samples collected from the sediment core RECORD 23 (Sardinia Channel) were analysed for
193 uranium and thorium isotopes to obtain absolute dating using a Thermo ScientificTM Neptune^{Plus} MC-ICPMS
194 installed at the Laboratoire des Sciences du Climat et de l'Environnement (LSCE, Gif-sur-Yvette, France). Prior
195 to analysis, the samples were carefully cleaned using a small diamond blade to remove any visible contamination
196 and sediment-filled cavities. The fragments were examined under a binocular microscope to ensure against the
197 presence of bioeroded zones and finally crushed into a coarse-grained powder with an agate mortar and pestle.
198 The powders (~60-100 mg) were transferred to acid cleaned Teflon beakers, ultrasonicated in MilliQ water,
199 leached with 0.1N HCl for ~ 15 s and finally rinsed twice with MilliQ water. The physically and chemically
200 cleaned samples were dissolved in 3-4 ml dilute HCl (~10%) and mixed with an internal triple spike with known
201 concentrations of ^{229}Th , ^{233}U and ^{236}U , calibrated against a Harwell Uraninite solution (HU-1) assumed to be at
202 secular equilibrium. The solutions were evaporated to dryness at 70°C, redissolved in 0.6 ml 3N HNO₃ and then
203 loaded into 500 μl columns packed with Eichrom UTEVA resin to isolate uranium and thorium from the other
204 major and trace elements of the carbonate matrix. The U and Th separation and purification followed a
205 procedure slightly modified from Douville et al. (2010). The U and Th isotopes were determined following the
206 protocol recently revisited at LSCE (Pons-Branchu et al., 2014). The $^{230}\text{Th}/\text{U}$ ages were calculated from

207 measured atomic ratios through iterative age estimation (Ludwig and Titterton, 1994), using the ^{230}Th , ^{234}U
208 and ^{238}U decay constants of Cheng et al. (2013) and Jaffey et al. (1971). Due to the low ^{232}Th concentration (< 1
209 ng/g; see Table 1), no correction was applied for the non-radiogenic ^{230}Th fraction.

210

211 3.2.2 Nd isotopic composition analyses on cold-water coral fragments

212 Sub-samples of the CWC fragments from the Sardinia Channel used for U-series dating in this study (Table 1) as
213 well as sub-samples of the twenty-five CWC fragments originating from the Alboran Sea, which were already
214 radiocarbon-dated by Fink et al. (2013) (Table 2), were used for further Nd isotopic composition analyses. The
215 fragments (350 to 600 mg) were subjected to a mechanical and chemical cleaning procedure. The visible
216 contaminations, such as Fe-Mn coatings and detrital particles, were carefully removed from the inner and
217 outermost surfaces of the coral skeletons using a small diamond blade. The physically cleaned fragments were
218 ultrasonicated for 10 min with 0.1 N ultra-clean HCl, followed by several MilliQ water rinses and finally
219 dissolved in 2.5 N ultraclean HNO_3 . Nd was separated from the carbonate matrix using Eichrom TRU and LN
220 resins, following the analytical procedure described in detail in Copard et al. (2010).

221 The $^{143}\text{Nd}/^{144}\text{Nd}$ ratios of all purified Nd fractions were analyzed using the ThermoScientific Neptune^{Plus} Multi-
222 Collector Inductively Coupled Plasma Mass Spectrometer (MC-ICP-MS) hosted at LSCE. The mass-
223 fractionation correction was made by normalizing $^{146}\text{Nd}/^{144}\text{Nd}$ to 0.7219 and applying an exponential law.
224 During each analytical session, samples were systematically bracketed with analyses of JNdi-1 and La Jolla
225 standard solutions, which are characterised by accepted values of 0.512115 ± 0.000006 (Tanaka et al., 2000) and
226 0.511855 ± 0.000007 (Lugmair et al., 1983), respectively. Standard JNdi-1 and La Jolla solutions were analysed
227 at concentrations similar to those of the samples (5-10 ppb) and all the measurements affected by instrumental
228 bias were corrected, when necessary, using La Jolla standard. The external reproducibility (2σ) for time resolved
229 measurement, deduced from repeated analyses of La Jolla and JNdi-1 standards, ranged from 0.1 to 0.5 ϵNd
230 units for the different analytical sessions. The analytical error for each sample analysis was taken as the external
231 reproducibility of the La Jolla standard for each session. Concentrations of Nd blanks were negligible compared
232 to the amount of Nd of CWC investigated in this study.

233

234 3.3. Analyses on sediment of core SU92-33

235 3.3.1. Radiocarbon dating

236 Radiocarbon dating was measured at UMS-ARTEMIS (Pelletron 3MV) AMS (CNRS-CEA Saclay, France).
237 Seven AMS radiocarbon (^{14}C) dating were performed in first 1.2 m of the core SU92-33 on well-preserved
238 calcareous tests of the planktonic foraminifera *G. bulloides* in the size fraction >150 μm (Table 3). The age
239 model for the core was derived from the calibrated planktonic ages by applying a mean reservoir effect of ~400
240 years (Siani et al., 2000, 2001). All ^{14}C ages were converted to calendar years (cal. yr BP, BP = AD 1950) by
241 using the INTCAL13 calibration data set (Reimer et al., 2013) and the CALIB 7.0 program (Stuiver and Reimer,
242 1993).

243

244 3.3.2. Stable isotopes

245 Stable oxygen ($\delta^{18}\text{O}$) and carbon ($\delta^{13}\text{C}$) isotope measurements were performed in core SU92-33 on well-
246 preserved (clean and intact) samples of the planktonic foraminifera *G. bulloides* (250-315 μm fraction) and the

247 epibenthic foraminifera *C. pachyderma* (250-315 μm fraction) using a Finnigan MAT-253 mass spectrometer at
248 the State Key Laboratory of Marine Geology (Tongji University). Both $\delta^{18}\text{O}$ and $\delta^{13}\text{C}$ values are presented
249 relative to the Pee Dee Belemnite (PDB) scale by comparison with the National Bureau of Standards (NBS) 18
250 and 19. The mean external reproducibility was checked by replicate analyses of laboratory standards and is better
251 than $\pm 0.07\text{‰}$ (1σ) for $\delta^{18}\text{O}$ and $\pm 0.04\text{‰}$ for $\delta^{13}\text{C}$.

252 3.3.3 *Nd isotope measurements on planktonic foraminifera*

253 Approximately 25 mg of mixed planktonic foraminifera species were picked from the $>63\ \mu\text{m}$ size fraction of
254 each sample already used for stable isotope measurements (Table 4). The samples were gently crushed between
255 glass slides under the microscope to ensure that all chambers were open, and ultrasonicated with MilliQ water.
256 Samples were allowed to settle between ultrasonication steps before removing the supernatant. Each sample was
257 rinsed thoroughly with MilliQ water until the solution was clear and free of clay. The cleaned samples were
258 dissolved in 1N acetic acid and finally centrifuged to ensure that all residual particles were removed, following
259 the procedure described in Roberts et al. (2010). Nd was separated following the analytical procedure reported in
260 Wu et al. (2015). For details on the measurement of Nd isotopes see the section above.

261

262 3.3.4. *Modern analogue technique (MAT)*

263 The palaeo-sea surface temperatures (SST) were estimated using the modern analogue technique (MAT)
264 (Hutson, 1980; Prell, 1985), implemented by Kallel et al. (1997) for the Mediterranean Sea. This method directly
265 measures the difference between the faunal composition of a fossil sample with a modern database, and it
266 identifies the best modern analogues for each fossil assemblage (Prell, 1985). Reliability of SST reconstructions
267 is estimated using a square chord distance test (dissimilarity coefficient), which represents the mean degree of
268 similarity between the sample and the best 10 modern analogues. When the dissimilarity coefficient is lower than
269 0.25, the reconstruction is considered to be of good quality (Overpeck et al., 1985; Kallel et al., 1997). For core
270 SU92-33, good dissimilarity coefficients are <0.2 , with an average value of ~ 0.13 (varying between 0.07 and
271 0.19) (Fig. 2a). The calculated mean standard deviation of SST estimates observed in core MD90-917 are ~ 1.5
272 $^{\circ}\text{C}$ from the late glacial period to the Younger Dryas and $\sim 1.2\ ^{\circ}\text{C}$ for the Holocene.

273

274 4. Results

275 4.1. *Cold-water corals*

276 The good state of preservation for the CWC samples from the Sardinia Channel (RECORD 23; Fig. 1) is attested
277 by their initial $\delta^{234}\text{U}$ values (Table 1), which is in the range of the modern seawater value (146.8 ± 0.1 ; Andersen
278 et al., 2010). If the uncertainty of the $\delta^{234}\text{U}_i$ is taken into account, all the values fulfill the so-called “strict” ± 4
279 $\%$ reliability criterion and the U/Th ages can be considered strictly reliable. The coral ages range from
280 0.091 ± 0.011 to 10.904 ± 0.042 ka BP (Table 1), and reveal three distinct clusters of coral age distribution during
281 the Holocene representing periods of sustained coral occurrence. These periods coincide with the Early Holocene
282 encompassing a 700-years-lasting time interval from ~ 10.9 to 10.2 ka BP, the very late Early Holocene at ~ 8.7
283 ka BP, and the Late Holocene starting at ~ 1.5 ka BP (Table 1).

284 Radiocarbon ages obtained for CWC samples collected in the Alboran Sea were published by Fink et al. (2013)
285 (Table 2). They also document three periods of sustained CWC occurrence coinciding with the Bølling–Allerød

286 (B-A) interstadial (13.5–12.9 cal ka BP), the Early Holocene (11.2–9.8 cal ka BP) and the Mid- to Late Holocene
287 (5.4–0.3 cal ka BP).

288 The ϵNd record obtained from the CWC samples from the Alboran Sea displays a narrow range from -9.22 ± 0.30
289 to -8.59 ± 0.3 , which is comparable to the ϵNd record of the planktonic foraminifera from the Balearic Sea over
290 the last 13.5 kyr (Table 2, Fig. 3b). Most of the CWC ϵNd values are similar within the analytical error and the
291 record does not reveal any clear difference over the last ~13.5 kyr.

292 On the contrary, the CWC samples from the Sardinia Channel display a relatively large ϵNd range, with values
293 varying from -5.99 ± 0.50 to -7.75 ± 0.10 during the Early and Late Holocene, and values as low as -8.66 ± 0.30
294 during the the mid-sapropel S1 deposition (S1a) at ~8.7 ka BP (Table 1, Fig. 3c).

295

296

297 **4.2 Core SU92-33**

298 The stratigraphy of core SU92-33 was derived from the $\delta^{18}\text{O}$ variations of the planktonic foraminifera
299 *G. bulloides* (Fig. 2b). The last glacial/interglacial transition and the Holocene encompasses the upper 2.1 m of
300 the core (Fig. 2b). The $\delta^{18}\text{O}$ record of *G. bulloides* shows higher values (~3.5 ‰) during the late glacial
301 compared to the Holocene (from ~1.5 to 0.8 ‰) exhibiting a pattern similar to those observed in nearby deep-sea
302 cores from the Western Mediterranean Sea (Sierro et al., 2005; Melki et al., 2009).

303 The age model for the upper 1.2 m of the core SU92-33 was based on 7 AMS- ^{14}C age measurements and a
304 linear interpolation between these ages (Table 3, Fig. 2). For the lower portion of the core, a control point was
305 established at the onset of the last deglaciation, which is coeval in the western and central Mediterranean Sea at
306 ~17 cal ka BP (Sierro et al., 2005; Melki et al., 2009; Siani et al., 2001). Overall, the upper 2.1 m of core SU92-
307 33 spans the last 19 kyr, with an estimated average sedimentation rate ranging from ~15 cm ka⁻¹ during the
308 deglaciation to ~10 cm ka⁻¹ during the Holocene.

309 April-May SST reconstruction was derived from MAT to define the main climatic events recorded in
310 core SU92-33 during the last 19 kyr. SST vary from 8.5°C to 17.5°C with high amplitude variability over the last
311 19 kyr BP (Fig. 2a). The LGM (19-18 ka BP) is characterized by SST values centered at around 12°C. Then, a
312 progressive decrease of ~4°C between 17.8 ka and 16 ka marks the Heinrich Stadial 1 (HS1) (Fig. 2a). A
313 warming phase (~14°C) between 14.5 ka BP and 13.8 ka BP coincides with the B-A interstadial and is followed
314 by a cooling (~11°C) between 13.1 ka BP and 11.8 ka BP largely corresponding to the YD (Fig. 2a). During the
315 Holocene, SST show mainly values of ~16°C, with one exception between 7 ka BP and 6 ka BP pointing to an
316 abrupt cooling of ~3°C (Fig. 2a). From the late glacial to the Holocene, SST variations show a similar pattern to
317 that previously observed in the Gulf of Lions and Tyrrhenian Sea (Kallel et al., 1997; Melki et al., 2009) as well
318 as in the Alboran Sea (Martrat et al., 2014; Rodrigo-Gámiz et al., 2014). They are globally synchronous for the
319 main climatic transitions to the well dated South Adriatic Sea core MD90-917 (Siani et al., 2004) confirming the
320 robustness of the SU92-33 age model (Fig. 2a).

321 The $\delta^{18}\text{O}$ and $\delta^{13}\text{C}$ records obtained from the benthic foraminifera *C. pachyderma* display significant variations
322 at millennial time scales (Figs. 2c and 2d). The $\delta^{18}\text{O}$ values decrease steadily from ~4.5 ‰ during the LGM to
323 ~1.5 ‰ during the Holocene, without showing any significant excursion during HS1 and the YD events (Fig.
324 2c), in agreement with results obtained from the neighbor core MD99-2343 (Sierro et al., 2005).

325 The $\delta^{13}\text{C}$ record of *C. pachyderma* shows a decreasing trend since the LGM with a low variability from ~ 1.6 ‰
326 to ~ 0.6 ‰ (Fig. 2d). The heaviest $\delta^{13}\text{C}$ values are related to the LGM (~ 1.6 ‰) while the lightest values (~ 0.6
327 ‰) characterize the Early Holocene and in particular the period corresponding to the sapropel S1 event in the
328 eastern Mediterranean basin (Fig. 2d).

329 The ϵNd values of planktonic foraminifera of core SU92-33 from the Balearic Sea vary within a relatively
330 narrow range between -9.50 ± 0.30 and -8.61 ± 0.30 , with an average value of -9.06 ± 0.28 (Table 2, Fig. 3b). The
331 record shows a slight increasing trend since the LGM, with the more unradiogenic values (average -9.28 ± 0.15 ;
332 $n=7$) being observed in the oldest part of the record (between 18 and 13.5 ka BP), whereas Holocene values are
333 generally more radiogenic (average -8.84 ± 0.22 ; $n=17$) (Fig. 3b).

334

335 5. Discussion

336 Overall, the CWC and foraminiferal ϵNd values measured in this study point to a pronounced dispersion at
337 intermediate depth in terms of absolute values and variability in Nd isotopes during the Holocene between the
338 Alboran and Balearic Seas and the Sardinia Channel. Furthermore, the foraminiferal ϵNd record reveals an
339 evolution towards more radiogenic values at intermediate water depth in the Balearic Sea over the last ~ 19 kyr
340 (Fig. 3).

341 A prerequisite to properly interpret such ϵNd differences and variations through time consists in characterizing
342 first the present-day ϵNd of the main water-mass end-members present in the western Mediterranean basin. It is
343 also necessary to evaluate the temporal changes in ϵNd of the end-members since the LGM and assess the
344 potential influences of lithogenic Nd input and regional exchange between the continental margins and seawater
345 (“boundary exchange”; Lacan and Jeandel, 2001, 2005) on the ϵNd values of intermediate water masses.

346 During its westward flow, the LIW continuously mixes with surrounding waters with different ϵNd signatures
347 lying above and below. For the western Mediterranean basin, these water masses are the MAW/Western
348 Intermediate Water (WIW) and the TDW/WMDW. As a result, a gradual ϵNd gradient exists at intermediate
349 depth between the eastern and western Mediterranean basins, with LIW values becoming progressively more
350 unradiogenic towards the Strait of Gibraltar, from -4.8 ± 0.2 at 227 m in the Levantine basin to -10.4 ± 0.2 at 200 m
351 in the Alboran Sea (Tachikawa et al., 2004). Such an ϵNd pattern implies an effective vertical mixing with more
352 unradiogenic water masses along the E-W LIW trajectory ruling out severe isotopic modifications of the LIW
353 due to the local exchange between the continental margins and seawater. Unfortunately, no information exists on
354 the potential temporal variability in ϵNd of the Mediterranean water-mass end-members since the LGM.

355 It has been demonstrated that eolian dust input can modify the surface and sub-surface ϵNd distribution of the
356 ocean in some areas (Arsouze et al., 2009). The last glacial period was associated with an aridification of North
357 Africa (Sarnthein et al., 1981; Hooghiemstra et al., 1987; Moreno et al., 2002; Wienberg et al., 2010) and higher
358 fluxes of Saharan dust to the NE tropical Atlantic (Itambi et al., 2009) and the western Mediterranean Sea
359 characterized by unradiogenic ϵNd values (between -11 ± 0.4 and -14 ± 0.4 ; see synthesis in Scheuvens et al.,
360 2013). Bout-Roumazelles et al. (2013) documented a dominant role of eolian supply in the Siculo-Tunisian
361 Strait during the last 20 ka, with the exception of a significant riverine contribution (from the Nile River) and a
362 strong reduction of eolian input during the sapropel S1 event. Such variations in the eolian input to the
363 Mediterranean Sea are not associated to a significant change in the seawater ϵNd record obtained for the Balearic
364 Sea (core SU92-33) during the sapropel S1 event (Fig. 3). Furthermore, the ϵNd signature of the CWC from the

365 Sardinia Channel (core RECORD 23) shifts to more unradiogenic values (-8.66 ± 0.30) during the sapropel S1
366 event, which is opposite to what would be expected from a strong reduction of eolian sediment input. In a recent
367 study, Rodrigo-Gámiz et al. (2015) have documented variations in the terrigenous provenance from a sediment
368 record in the Alboran Sea (core 293G; $36^{\circ}10.414'N$, $2^{\circ}45.280'W$, 1840 m water depth) since the LGM.
369 Radiogenic isotopes (Sr, Nd, Pb) point to changes from North African dominated sources during the glacial
370 period to European dominated source during the Holocene. Nevertheless, the major Sr-Nd-Pb excursions
371 documented by Rodrigo-Gámiz et al. (2015) and dated at ca. 11.5, 10.2, 8.9-8.7, 5.6, 2.2 and 1.1. ka cal BP do
372 not seem to affect the ϵNd values of our foraminifera and coral records.
373 Taken together, these results suggest that changes of eolian dust input since the LGM cannot explain the
374 observed ϵNd variability at intermediate water depths.
375 Consequently, assuming that the Nd isotopic budget of the western Mediterranean Sea has not been strongly
376 modified since the LGM, the reconstructed variations of the E-W gradient of ϵNd values in the western
377 Mediterranean Sea for the past and notably during the sapropel S1 event (Fig. 3) are indicative of a major
378 reorganization of intermediate water circulation.

379

380 ***5.1 Hydrological changes in the Alboran and Balearic Seas since the LGM***

381 The range in ϵNd for the CWC from the Alboran Sea (from -9.22 ± 0.30 to $-8.8.59 \pm 0.30$; Table 2) is very close to
382 the one obtained for the planktonic foraminifera from the Balearic Sea (from -9.50 ± 0.30 to -8.61 ± 0.30 ; Table 4,
383 Fig. 3c), suggesting that both sites are influenced by the same intermediate water masses at least for the last 13.5
384 kyr BP. Today, LIW occupies a depth range between ~ 200 and ~ 700 m in the western Mediterranean basin
385 (Millot, 1999; Sparnocchia et al., 1999). More specifically, the salinity maximum corresponding to the core of
386 LIW is found at around 400 m in the Alboran Sea (Millot, 2009) and up to 550 m in the Balearic Sea (López-
387 Jurado et al., 2008). The youngest CWC sample collected in the Alboran Sea with a rather "recent" age of 0.34
388 cal ka BP (Fink et al. 2013) displays an ϵNd value of -8.59 ± 0.30 (Table 2) that is similar to the present-day value
389 of the LIW at the same site (-8.3 ± 0.2) (Dubois-Dauphin et al., submitted) and is significantly different from the
390 WMDW ϵNd signature in the Alboran Sea (-10.7 ± 0.2 , 1270 m water depth; Tachikawa et al., 2004). Considering
391 the intermediate depth range of the studied CWC and foraminifera samples, we can reasonably assume that
392 samples from both sites, in the Balearic Sea (622 m water depth) and in the Alboran Sea (280 to 442 m water
393 depth), record ϵNd variations of the LIW. The ϵNd record obtained from planktonic foraminifera generally
394 displays more unradiogenic and homogenous values before ~ 13 cal ka BP (range from -9.46 to -9.12) compared
395 to the most recent part of the record (range from -9.50 to -8.61), with the highest value of -8.61 ± 0.3 in the Early
396 and Late Holocene.

397 The SST record displays values centered at around $12^{\circ}C$ during the LGM with a subsequent rapid SST decrease
398 towards $9^{\circ}C$, highlighting the onset of the HS1 (Fig. 2a). These values are well comparable to recent high-
399 resolution SST data obtained in the Alboran Sea (Martrat et al., 2014; Rodrigo-Gámiz et al., 2014).

400 The $\delta^{18}O$ record obtained on *G. bulloides* indicates an abrupt 1‰ excursion towards lighter values centered at
401 about 16 cal ka BP (Table 4), synchronous with the HS1 (Fig. 2b), which is similar to the $\delta^{18}O$ shift reported by
402 Sierro et al. (2005) for a core collected at 2391 m water depth NE of the Balearic Islands (MD99-2343; Fig. 1).
403 As the Heinrich events over the last glacial period are characterized by colder and fresher surface water in the
404 Alboran Sea (Cacho et al., 1999; Pérez-Folgado et al., 2003; Martrat et al., 2004, 2014; Rodrigo-Gámiz et al.,

405 2014) and dry climate on land over the western Mediterranean Sea (Allen et al., 1999; Combourieu-Nebout et
406 al., 2002; Sanchez Goni et al., 2002; Bartov et al., 2003), lighter $\delta^{18}\text{O}$ values of planktonic *G. bulloides* are
407 thought to be the result of the inflow of freshwater derived from the melting of icebergs in the Atlantic Ocean
408 into the Mediterranean Sea (Sierro et al., 2005; Rogerson et al., 2008).

409 During this time interval, the $\delta^{13}\text{C}$ record of *C. pachyderma* from the Balearic Sea (core SU92-33) displays a
410 decreasing $\delta^{13}\text{C}$ trend after ~16 cal ka BP (from 1.4 ‰ to 0.9 ‰; Table 4; Fig. 4a). Moreover, the $\delta^{13}\text{C}$ record
411 obtained on benthic foraminifera *C. pachyderma* from the deep Balearic Sea (core MD99-2343) reveals similar
412 $\delta^{13}\text{C}$ values before ~16 cal ka BP suggesting well-mixed and ventilated water masses during the LGM and the
413 onset of the deglaciation (Sierro et al., 2005).

414 The slightly lower foraminiferal ϵNd values before ~13 cal ka BP could reflect a stronger influence of water
415 masses deriving from the Gulf of Lions as WMDW (ϵNd : -9.4 ± 0.9 ; Henry et al., 1994; Tachikawa et al., 2004;
416 Montagna, pers. comm., 2016). This is in agreement with ϵNd results obtained by Jiménez-Espejo et al. (2015)
417 from planktonic foraminifera collected from deep-water sites (1989 m and 2382 m) in the Alboran Sea (Fig. 4c).
418 Jiménez-Espejo et al. (2015) documented lower ϵNd values (ranging from -10.14 ± 0.27 to -9.58 ± 0.22) during the
419 LGM, suggesting an intense deep-water formation. This is also associated to an enhanced activity of the deeper
420 branch of the MOW in the Gulf of Cádiz (Rogerson et al., 2005; Voelker et al., 2006) linked to the active
421 production of the WMDW in the Gulf of Lions during the LGM (Jiménez-Espejo et al., 2015).

422 The end of the HS1 (14.7 cal ka BP) is concurrent with the onset of the B-A warm interval characterized by
423 increased SST up to 14°C in the Balearic Sea (SU92-33; Fig. 3a), also identified for various sites in the
424 Mediterranean Sea (Cacho et al., 1999; Martrat et al., 2004, 2014; Essallami et al., 2007; Rodrigo-Gámiz et al.,
425 2014). The B-A interval is associated with the so-called melt-water pulse 1A (e.g. Weaver et al., 2003) occurring
426 at around 14.5 cal ka BP. This led to a rapid sea-level rise of about 20 m in less than 500 years and large
427 freshwater discharges in the Atlantic Ocean due to the melting of continental ice sheets (Deschamps et al., 2012),
428 resulting in an enhanced Atlantic inflow across the Strait of Gibraltar. Synchronously, cosmogenic dating of
429 Alpine glacier retreat throughout the western Mediterranean hinterland suggests maximum retreat rates (Ivy-
430 Ochs et al., 2007; Kelly et al., 2006). Overall, these events are responsible for freshening Mediterranean waters
431 and reduced surface water density, and hence, weakened ventilation of intermediate (Toucanne et al., 2012) and
432 deep-water masses (Cacho et al., 2000; Sierro et al., 2005). Similarly, lower benthic $\delta^{13}\text{C}$ values obtained for the
433 Balearic Sea (Fig. 4a) point to less ventilated intermediate water relative to the late glacial. In addition, a
434 decoupling in the benthic $\delta^{13}\text{C}$ values is observed between deep (MD99-2343) and intermediate (core SU92-33)
435 waters after ~16 cal ka BP (Sierro et al. 2005), suggesting an enhanced stratification of the water masses (Fig.
436 4a). At this time, the shallowest ϵNd record from the deep Alboran Sea (core 300G) shifted towards more
437 radiogenic values, while the deepest one (core 304G) remained close to the LGM values (Jimenez-Espejo et al.,
438 2015) (Fig. 4c). Furthermore, results from the UP10 fraction (particles $> 10 \mu\text{m}$) of the MD99-2343 sediment
439 core (Fig. 4d) indicate a declining bottom-current velocity at 15 ka BP (Frigola et al., 2008). Rogerson et al.
440 (2008) have hypothesized that during deglacial periods the sinking depth of dense waters produced in the Gulf of
441 Lions was shallower resulting in new intermediate water (WIW) rather than new deep-water (WMDW) as
442 observed today during mild winters (Millot, 1999; Schott et al., 1996). Therefore, intermediate depths of the
443 Balearic Sea could have been isolated from the deep-water with the onset of the T1 (at ~15 ka BP). The reduced
444 convection in the deep western Mediterranean Sea together with the shoaling of the nutricline (Rogerson et al.,

445 2008) led to the deposition of the ORL 1 (14.5 to 8.2 ka B.P; Cacho et al., 2002) and dysoxic conditions below
446 2000 m in agreement with the absence of epibenthic foraminifera such as *C. pachyderma* after 11 cal ka BP in
447 MD99-2343 (Sierro et al., 2005) (Fig. 4a).

448 After 13.5 ka BP, planktonic foraminifera ϵNd values from the Balearic Sea (core SU92-33) become more
449 radiogenic and are in the range of CWC ϵNd values from the Alboran Sea (Fig. 4b). These values may reveal a
450 stronger influence of the LIW in the Balearic Sea during the Younger Dryas, as also supported by the sortable
451 silt record from the Tyrrhenian Sea (Toucanne et al., 2012) (Fig. 4e). Deeper depths of the Alboran Sea also
452 record a stronger influence of the LIW with an ϵNd value of -9.1 ± 0.4 (Jimenez-Espejo et al., 2015). In addition,
453 a concomitant activation of the upper MOW branch, as reconstructed from higher values of Zr/Al ratio in
454 sediments of the Gulf of Cádiz, can be related to the enhanced LIW flow in the western Mediterranean Sea (Fig.
455 4f) (Bahr et al., 2015).

456 The time of sapropel S1 deposition (10.2 – 6.4 ka) is characterized by a weakening or a shutdown of
457 intermediate- and deep-water formation in the eastern Mediterranean basin (Rossignol-Strick et al., 1982; Cramp
458 and O’Sullivan, 1999; Emeis et al., 2000; Rohling et al., 2015). At this time, planktonic foraminifera ϵNd values
459 from intermediate water depths in the Balearic Sea (core SU92-33) remain high (between -9.15 ± 0.3 and -
460 8.61 ± 0.3) (Fig. 4b). On the other hand, the deeper Alboran Sea provides a value of -9.8 ± 0.3 pointing to a
461 stronger contribution of WMDW (Jimenez-Espejo et al., 2015), coeval with the recovery of deep-water activity
462 from core MD99-2343 (Frigola et al., 2008).

463

464

5.2 Hydrological changes in the Sardinia Channel during the Holocene

465 The present-day hydrographic structure of the Sardinia Channel is characterized by four water masses, with the
466 surface, intermediate and deep-water masses being represented by MAW, LIW and TDW/WMDW, respectively
467 (Astraldi et al., 2002a; Millot and Taupier-Lepage, 2005). In addition, the WIW, flowing between the MAW and
468 the LIW, has also been observed along the Channel (Sammari et al., 1999). The core of the LIW is located at
469 400-450 m water depth in the Tyrrhenian Sea (Hopkins, 1988; Astraldi et al., 2002b), which is the depth range of
470 CWC samples from the Sardinia Channel (RECORD 23; 414 m) (Taviani et al., 2015). The youngest CWC
471 sample dated at ~ 0.1 ka BP has an ϵNd value of -7.70 ± 0.10 (Table 1, Fig. 5), which is similar within error to the
472 value obtained from a seawater sample collected at 451 m close to the coral sampling location (-8.0 ± 0.4 ;
473 Montagna, pers. comm., 2016).

474 The CWC dating from the Sardinia Channel shows three distinct periods of sustained coral occurrence in this
475 area during the Holocene, with each displaying a large variability in ϵNd values. CWC from the Early Holocene
476 (10.9-10.2 ka BP) and the Late Holocene (<1.5 ka BP) exhibit similar ranges of ϵNd values (ranging from -
477 5.99 ± 0.50 to -7.75 ± 0.20 ; Table 1, Fig 5c). Such variations are within the present-day ϵNd range being
478 characteristic for intermediate waters in the eastern Mediterranean Sea (-6.6 ± 1.0 ; Tachikawa et al., 2004; Vance
479 et al., 2004). However, the CWC ϵNd values are more radiogenic than those observed at mid-depth in the
480 present-day western basin (ranging from -10.4 ± 0.2 to -7.58 ± 0.47 ; Henry et al., 1994; Tachikawa et al., 2004;
481 Montagna, pers. comm., 2016), suggesting a stronger LIW component in the Sardinia Channel during the Early
482 and Late Holocene. The Sardinian CWC ϵNd variability also reflects the sensitivity of the LIW to changes in the
483 eastern basin such as rapid variability of the Nile River flood discharge (Revel et al., 2014; 2015; Weldeab et al.,
484 2014) or a modification through time in the proportion between the LIW and the Cretan Intermediate Water

485 (CIW). Today, the intermediate water outflowing from the Strait of Sicily is composed by ~66 to 75 % of LIW
486 and 33 to 25 % of CIW (Manca et al., 2006; Millot, 2014). As the CIW is formed in the Aegean Sea, this
487 intermediate water mass is generally more radiogenic than LIW (Tachikawa et al., 2004; Montagna, pers.
488 comm., 2016). Following this hypothesis, a modification of the mixing proportion between the CIW and the
489 LIW may potentially explain values as radiogenic as about -6 in the Sardinia Channel during the Early and Late
490 Holocene (Fig. 5c). However, a stronger LIW and/or a CIW contribution cannot be responsible for ϵNd values as
491 low as -8.66 ± 0.30 observed during the sapropel S1 event at 8.7 ka BP (Table 1, Fig. 5c). Considering that such
492 unradiogenic value is not observed at intermediate depth in the modern eastern Mediterranean basin, the most
493 plausible hypothesis suggested here is that the CWC were influenced by a higher contribution of intermediate
494 water from the western basin.

495

496 *5.3 Hydrological implications for the intermediate water masses of the western Mediterranean Sea*

497 The ϵNd records of the Balearic Sea, Alboran Sea and Sardinia Channel document a temporal variability of the
498 east-west gradient in the western Mediterranean basin during the Holocene. The magnitude of the gradient
499 ranges from ~1.5 to ~3 ϵ units during the Early and Late Holocene and it is strongly reduced at 8.7 ka BP (from
500 0 to ~0.5 ϵ unit), coinciding with the sapropel S1 event affecting the eastern Mediterranean basin (Fig. 5). Such
501 variations could be the result of a modification of the Nd isotopic composition of intermediate water masses due
502 to changes of the LIW production through time and a higher contribution of the western-sourced intermediate
503 water towards the Sardinia Channel coinciding with the sapropel S1 event.

504 The LIW acquires its radiogenic ϵNd signature in the Mediterranean Levantine basin mainly from Nd exchange
505 between seawater and lithogenic particles originating mainly from Nile River (Tachikawa et al., 2004). A higher
506 sediment supply from the Nile River starting at ~15 ka BP was documented by a shift to more radiogenic ϵNd
507 values of the terrigenous fraction obtained from a sediment core having been influenced by the Nile River
508 discharge (Revel et al., 2015) (Fig. 5e). Others studies pointed to a gradual enhanced Nile River runoff as soon
509 as 14.8 ka BP and a peak of Nile discharge from 9.7 to 8.4 ka recorded by large increase in sedimentation rate
510 from 9.7 to 8.4 ka (>120 cm/ka) (Revel et al., 2015; Weldeab et al., 2014; Castaneda et al., 2016). Similarly,
511 enhanced Nile discharge at ~9.5 cal kyr B.P was inferred based on $\delta^{18}\text{O}$ in planktonic foraminifera from a
512 sediment core in the southeast Levantine Basin (PS009PC (32°07.7'N, 34°24.4'E; 552 m water depth)
513 (Hennekam et al., 2014). This increasing contribution of the Nile River to the eastern Mediterranean basin has
514 been related to the African Humid Period (14.8–5.5 ka BP; Shanahan et al., 2015), which in turn was linked to
515 the precessional increase in Northern Hemisphere insolation during low eccentricity (deMenocal et al., 2000;
516 Barker et al., 2004; Garcin et al., 2009). An increasing amount of radiogenic sediments dominated by the
517 Blue/Atbara Nile River contribution (Revel et al., 2014) could have modified the ϵNd of surface water towards
518 more radiogenic values (Revel, pers. comm., 2016). Indeed, planktonic foraminifera ϵNd values as high as ~ -3
519 have been documented in the eastern Levantine Basin (ODP site 967; 34°04.27'N, 32°43.53'E; 2553 m water
520 depth) during the sapropel S1 event as a result of enhanced Nile flooding (Scrivner et al., 2004). The radiogenic
521 signature was likely transferred to intermediate depth as a consequence of the LIW formation in the Rhodes
522 Gyre, and it might have been propagated westwards towards the Sardinia Channel.

523 Therefore, considering the more unradiogenic value of the CWC samples from the Sardinia Channel during the
524 sapropel S1a event, it is very unlikely that eastern-sourced water flowed at intermediate depth towards the

525 Sardinia Channel. A possible explanation could be the replacement of the radiogenic LIW that was no longer
526 produced in the eastern basin (Rohling, 1994) by less radiogenic western intermediate water (possibly WIW).
527 Such a scenario could even support previous hypotheses of a potential circulation reversal in the eastern
528 Mediterranean from anti-estuarine to estuarine during sapropel formation (Huang and Stanley, 1972; Calvert,
529 1983; Sarmiento et al., 1988; Buckley and Johnson, 1988; Thunell and Williams, 1989). An alternative
530 hypothesis would be that reduced surface water densities in the eastern Mediterranean during sapropel S1
531 resulted in the LIW sinking to shallower depths than at present. In this case, CWC from the Sardinia Channel
532 would have been bathed by underlying Western Intermediate Water during the sapropel S1a event.

533

534 **6. Conclusions**

535 The foraminiferal ϵNd record from intermediate depths in the Balearic Sea reveals a relatively narrow range of
536 ϵNd values varying between -9.50 and -8.61 since the LGM (~20 ka). Between 18 and 13.5 cal ka BP, the more
537 unradiogenic ϵNd values support a vigorous deep overturning in the Gulf of Lions while $\delta^{18}\text{O}$ and $\delta^{13}\text{C}$ values
538 indicate a stratification of the water masses after 16 cal ka BP. The stratification together with a decrease of the
539 deep-water intensity led to more radiogenic values after ~13 cal ka BP. The foraminiferal ϵNd record, supported
540 by ϵNd values from CWC in the Alboran Sea, shows only minor changes in neodymium isotopes from 13.5 cal
541 ka BP to 0.34 cal ka BP, suggesting that the westernmost part of the western Mediterranean basin is not very
542 sensitive to hydrological variations of the LIW.

543 On the contrary, CWC located at the depth of the LIW in the Sardinia Channel exhibit large ϵNd variations
544 (between -7.75 ± 0.10 and -5.99 ± 0.50) during the Holocene, suggesting either the role of the Nile River in
545 changing the ϵNd of the LIW in the eastern Mediterranean basin or a variable LIW/CIW mixing of the water
546 outflowing from the Strait of Sicily. At the time of the sapropel S1 event at ~8.7 ka BP, CWC display a shift
547 toward lower values (-8.66 ± 0.30), similar to those found at intermediate depths in the westernmost part of the
548 western basin. This suggests that western-sourced intermediate water likely filled mid-depth of the southern
549 Sardinia, replacing LIW that was no longer produced (or heavily reduced) in the eastern basin. These results
550 could potentially support a reversal of the Mediterranean circulation, although this assumption needs further
551 investigation to be confirmed.

552

553 **Acknowledgements**

554 The research leading to this study has received funding from the MISTRALS/PALEOMEX/COFIMED, the
555 French National Research Agency "Investissement d'Avenir" (n°ANR-10-LABX-0018), the HAMOC project
556 ANR-13-BS06-0003 and ENVIMED/Boron Isotope and Trace Elements project. This work contributes to the
557 RITMARE project. We thank Hiske Fink for selecting and kindly providing the cold-water corals samples from
558 the Alboran Sea. We further thank François Thil and Louise Bordier for their support with Nd isotopic
559 composition analyses. Paolo Montagna is grateful for financial support from the Short Term Mobility Program
560 (CNR). Thanks are also extended to the captains, crews, chief scientists, and scientific parties of research cruises
561 RECORD (R/V Urania), POS-385 (R/V Poseidon) and PALEOCINAT II (R/V Le Suroît).

562

563 **References**

- 564 Abu-Zied, R. H., Rohling, E. J., Jorissen, F. J., Fontanier, C., Casford, J. S. L. and Cooke, S.: Benthic
565 foraminiferal response to changes in bottom-water oxygenation and organic carbon flux in the eastern
566 Mediterranean during LGM to Recent times, *Mar. Micropaleontol.*, 67(1-2), 46–68,
567 doi:10.1016/j.marmicro.2007.08.006, 2008.
- 568 Allen, J. R. M., Huntley, B., Brandt, U., Brauer, A., Hubberten, H., Keller, J., Kraml, M., Mackensen, A.,
569 Mingram, J., Negendank, J. F. W., Nowaczyk, N. R., Oberhänsli, H., Watts, W. A., Wulf, S. and Zolitschka, B.:
570 Rapid environmental changes in southern Europe during the last glacial period, *Nature*, 400(6746), 740–743,
571 doi:10.1038/23432, 1999.
- 572 Andersen, M. B., Stirling, C. H., Zimmermann, B. and Halliday, A. N.: Precise determination of the open ocean
573 ²³⁴U/²³⁸U composition, *Geochemistry, Geophys. Geosystems*, 11(12), Q12003, doi:10.1029/2010GC003318,
574 2010.
- 575 Arsouze, T., Dutay, J.-C., Lacan, F. and Jeandel, C.: Reconstructing the Nd oceanic cycle using a coupled
576 dynamical – biogeochemical model, *Biogeosciences*, 6(12), 2829–2846, doi:10.5194/bg-6-2829-2009, 2009.
- 577 Astraldi, M., Gasparini, G. P., Gervasio, L. and Salusti, E.: Dense Water Dynamics along the Strait of Sicily
578 (Mediterranean Sea), *J. Phys. Oceanogr.*, 31(12), 3457–3475, doi:10.1175/1520-
579 0485(2001)031<3457:DWDATS>2.0.CO;2, 2001.
- 580 Astraldi, M., Gasparini, G. P., Vetrano, A. and Vignudelli, S.: Hydrographic characteristics and interannual
581 variability of water masses in the central Mediterranean: A sensitivity test for long-term changes in the
582 Mediterranean Sea, *Deep. Res. Part I Oceanogr. Res. Pap.*, 49(4), 661–680, doi:10.1016/S0967-0637(01)00059-
583 0, 2002a.
- 584 Astraldi, M., Conversano, F., Civitarese, G., Gasparini, G. P., Ribera d’Alcalà, M. and Vetrano, a.: Water mass
585 properties and chemical signatures in the central Mediterranean region, *J. Mar. Syst.*, 33-34, 155–177,
586 doi:10.1016/S0924-7963(02)00057-X, 2002b.
- 587 Bahr, A., Kaboth, S., Jiménez-Espejo, F. J., Sierro, F. J., Voelker, A. H. L., Lourens, L., Röhl, U., Reichert, G.
588 J., Escutia, C., Hernández-Molina, F. J., Pross, J. and Friedrich, O.: Persistent monsoonal forcing of
589 Mediterranean Outflow Water dynamics during the late Pleistocene, *Geology*, 43(11), 951–954,
590 doi:10.1130/G37013.1, 2015.
- 591 Barker, P. A., Talbot, M. R., Street-Perrott, F. A., Marret, F., Scourse, J. and Odada, E. O.: Late Quaternary
592 climatic variability in intertropical Africa, in *Past Climate Variability through Europe and Africa*, pp. 117–138,
593 Springer Netherlands, Dordrecht., 2004.
- 594 Bartov, Y., Goldstein, S. L., Stein, M. and Enzel, Y.: Catastrophic arid episodes in the Eastern Mediterranean
595 linked with the North Atlantic Heinrich events, *Geology*, 31(5), 439, doi:10.1130/0091-
596 7613(2003)031<0439:CAEITE>2.0.CO;2, 2003.

- 597 Bigg, G. R. and Wadley, M. R.: Millennial-scale variability in the oceans: an ocean modelling view, *J. Quat.*
598 *Sci.*, 16(4), 309–319, doi:10.1002/jqs.599, 2001.
- 599 Bout-Roumazeilles, V., Combourieu-Nebout, N., Desprat, S., Siani, G., Turon, J. L. and Essallami, L.: Tracking
600 atmospheric and riverine terrigenous supplies variability during the last glacial and the Holocene in central
601 Mediterranean, *Clim. Past*, 9(3), 1065–1087, doi:10.5194/cp-9-1065-2013, 2013.
- 602 Buckley, H. A. and Johnson, L. R.: Late pleistocene to recent sediment deposition in the central and western
603 Mediterranean, *Deep Sea Res. Part A. Oceanogr. Res. Pap.*, 35(5), 749–766, doi:10.1016/0198-0149(88)90028-
604 3, 1988.
- 605 Cacho, I., Pelejero, C., Grimalt, J. O., Calafat, A. and Canals, M.: C37 alkenone measurements of sea surface
606 temperature in the Gulf of Lions (NW Mediterranean), *Org. Geochem.*, 30(7), 557–566, doi:10.1016/S0146-
607 6380(99)00038-8, 1999.
- 608 Cacho, I., Grimalt, J. O., Sierro, F. J., Shackleton, N. and Canals, M.: Evidence for enhanced Mediterranean
609 thermohaline circulation during rapid climatic coolings, *Earth Planet. Sci. Lett.*, 183(3-4), 417–429,
610 doi:10.1016/S0012-821X(00)00296-X, 2000.
- 611 Cacho, I., Grimalt, J. O., Canals, M., Sbaiffi, L., Shackleton, N. J., Schönfeld, J. and Zahn, R.: Variability of the
612 western Mediterranean Sea surface temperature during the last 25,000 years and its connection with the Northern
613 Hemisphere climatic changes, *Paleoceanography*, 16(1), 40–52, doi:10.1029/2000PA000502, 2001.
- 614 Cacho, I., Grimalt, J. O. and Canals, M.: Response of the Western Mediterranean Sea to rapid climatic variability
615 during the last 50,000 years: a molecular biomarker approach, *J. Mar. Syst.*, 33-34, 253–272,
616 doi:10.1016/S0924-7963(02)00061-1, 2002.
- 617 Cacho, I., Shackleton, N., Elderfield, H., Sierro, F. J. and Grimalt, J. O.: Glacial rapid variability in deep-water
618 temperature and $\delta^{18}\text{O}$ from the Western Mediterranean Sea, *Quat. Sci. Rev.*, 25(23-24), 3294–3311,
619 doi:10.1016/j.quascirev.2006.10.004, 2006.
- 620 Calvert, S. E.: Geochemistry of Pleistocene sapropels and associated sediments from the Eastern Mediterranean,
621 *Oceanol. Acta*, 6(3), 255–267, 1983.
- 622 Castañeda, I. S., Schouten, S., Pätzold, J., Lucassen, F., Kasemann, S., Kuhlmann, H. and Schefuß, E.:
623 Hydroclimate variability in the Nile River Basin during the past 28,000 years, *Earth Planet. Sci. Lett.*, 438, 47–
624 56, doi:10.1016/j.epsl.2015.12.014, 2016.
- 625 Cheng, H., Lawrence Edwards, R., Shen, C.-C., Polyak, V. J., Asmerom, Y., Woodhead, J. D., Hellstrom, J.,
626 Wang, Y., Kong, X., Spötl, C., Wang, X. and Calvin Alexander, E.: Improvements in ^{230}Th dating, ^{230}Th and
627 ^{234}U half-life values, and U–Th isotopic measurements by multi-collector inductively coupled plasma mass
628 spectrometry, *Earth Planet. Sci. Lett.*, 371-372, 82–91, doi:10.1016/j.epsl.2013.04.006, 2013.
- 629 Colin, C., Frank, N., Copard, K. and Douville, E.: Neodymium isotopic composition of deep-sea corals from the
630 NE Atlantic: implications for past hydrological changes during the Holocene, *Quat. Sci. Rev.*, 29(19-20), 2509–

631 2517, doi:10.1016/j.quascirev.2010.05.012, 2010.

632 Combourieu-Nebout, N., Turon, J. L., Zahn, R., Capotondi, L., Londeix, L. and Pahnke, K.: Enhanced aridity
633 and atmospheric high-pressure stability over the western Mediterranean during the North Atlantic cold events of
634 the past 50 k.y, *Geology*, 30(10), 863–866, doi:10.1130/0091-7613(2002)030<0863:EAAAHP>2.0.CO;2, 2002.

635 Copard, K., Colin, C., Douville, E., Freiwald, A., Gudmundsson, G., De Mol, B. and Frank, N.: Nd isotopes in
636 deep-sea corals in the North-eastern Atlantic, *Quat. Sci. Rev.*, 29(19-20), 2499–2508,
637 doi:10.1016/j.quascirev.2010.05.025, 2010.

638 Copard, K., Colin, C., Henderson, G. M., Scholten, J., Douville, E., Sicre, M.-A. and Frank, N.: Late Holocene
639 intermediate water variability in the northeastern Atlantic as recorded by deep-sea corals, *Earth Planet. Sci. Lett.*,
640 313-314, 34–44, doi:10.1016/j.epsl.2011.09.047, 2012.

641 Cramp, A. and O’Sullivan, G.: Neogene sapropels in the Mediterranean: a review, *Mar. Geol.*, 153(1-4), 11–28,
642 doi:10.1016/S0025-3227(98)00092-9, 1999.

643 De Lange, G. J., Thomson, J., Reitz, A., Slomp, C. P., Principato, M. S., Erba, E. and Corselli, C.: Synchronous
644 basin-wide formation and redox-controlled preservation of a Mediterranean sapropel, *Nat. Geosci.*, 1(9), 606–
645 610, 2008.

646 DeMenocal, P., Ortiz, J., Guilderson, T. and Sarnthein, M.: Coherent High- and Low-Latitude Climate
647 Variability During the Holocene Warm Period, *Science* (80-.), 288(5474), 2198–2202,
648 doi:10.1126/science.288.5474.2198, 2000.

649 Deschamps, P., Durand, N., Bard, E., Hamelin, B., Camoin, G., Thomas, A. L., Henderson, G. M., Okuno, J. and
650 Yokoyama, Y.: Ice-sheet collapse and sea-level rise at the Bølling warming 14,600 years ago, *Nature*,
651 483(7391), 559–564, doi:10.1038/nature10902, 2012.

652 Douville, E., Sallé, E., Frank, N., Eisele, M., Pons-Branchu, E. and Ayrault, S.: Rapid and accurate U–Th dating
653 of ancient carbonates using inductively coupled plasma-quadrupole mass spectrometry, *Chem. Geol.*, 272(1-4),
654 1–11, doi:10.1016/j.chemgeo.2010.01.007, 2010.

655 Dubois-Dauphin, Q., Colin, C., Bonneau, L., Montagna, P., Wu, Q., Van Rooij, D., Reverdin, G., Douville, E.,
656 Thil, F., Waldner, A., Frank, N.: Fingerprinting North-east Atlantic water masses using Neodymium isotopes,
657 *GCA*, submitted.

658

659 Elmore, A. C., Piotrowski, A. M., Wright, J. D. and Scrivner, A. E.: Testing the extraction of past seawater Nd
660 isotopic composition from North Atlantic deep sea sediments and foraminifera, *Geochemistry, Geophys.*
661 *Geosystems*, 12(9), doi:10.1029/2011GC003741, 2011.

662 Emeis, K.-C., Sakamoto, T., Wehausen, R. and Brumsack, H.-J.: The sapropel record of the eastern
663 Mediterranean Sea — results of Ocean Drilling Program Leg 160, *Palaeogeogr. Palaeoclimatol. Palaeoecol.*,
664 158(3-4), 371–395, doi:10.1016/S0031-0182(00)00059-6, 2000.

665 Fink, H. G., Wienberg, C., De Pol-Holz, R., Wintersteller, P. and Hebbeln, D.: Cold-water coral growth in the
666 Alboran Sea related to high productivity during the Late Pleistocene and Holocene, *Mar. Geol.*, 339, 71–82,
667 doi:10.1016/j.margeo.2013.04.009, 2013.

668 Frigola, J., Moreno, A., Cacho, I., Canals, M., Sierro, F. J., Flores, J. a., Grimalt, J. O., Hodell, D. a. and Curtis,
669 J. H.: Holocene climate variability in the western Mediterranean region from a deepwater sediment record,
670 *Paleoceanography*, 22(2), n/a–n/a, doi:10.1029/2006PA001307, 2007.

671 Frigola, J., Moreno, A., Cacho, I., Canals, M., Sierro, F. J., Flores, J. A. and Grimalt, J. O.: Evidence of abrupt
672 changes in Western Mediterranean Deep Water circulation during the last 50kyr: A high-resolution marine
673 record from the Balearic Sea, *Quat. Int.*, 181(1), 88–104, doi:10.1016/j.quaint.2007.06.016, 2008.

674 Garcin, Y., Junginger, A., Melnick, D., Olago, D. O., Strecker, M. R. and Trauth, M. H.: Late Pleistocene–
675 Holocene rise and collapse of Lake Suguta, northern Kenya Rift, *Quat. Sci. Rev.*, 28(9-10), 911–925,
676 doi:10.1016/j.quascirev.2008.12.006, 2009.

677 Hebbeln, D., Wienberg, C., Beuck, L., Freiwald, A., Wintersteller, P. and cruise participants (2009) Report and
678 preliminary results of R/V POSEIDON Cruise 385 "Cold-water corals of the Alboran Sea (western
679 Mediterranean Sea)", Faro - Toulon, 29.5. - 16.6.2009. Reports of the Department of Geosciences at the
680 University of Bremen, No. 273. Department of Geosciences, Bremen University. urn:nbn:de:gbv:46-
681 ep000106508.

682 Hennekam, R., Jilbert, T., Schnetger, B. and De Lange, G. J.: Solar forcing of Nile discharge and sapropel S1
683 formation in the early to middle Holocene eastern Mediterranean, *Paleoceanography*, 29(5), 343–356,
684 doi:10.1002/2013PA002553, 2014.

685 Henry, F., Jeandel, C., Dupré, B. and Minster, J.-F.: Particulate and dissolved Nd in the western Mediterranean
686 Sea: Sources, fate and budget, *Mar. Chem.*, 45(4), 283–305, doi:10.1016/0304-4203(94)90075-2, 1994.

687 Hooghiemstra, H., Bechler, A. and Beug, H.-J.: Isopollen maps for 18,000 years B.P. of the Atlantic offshore of
688 northwest Africa: Evidence for paleowind circulation, *Paleoceanography*, 2, 561–582,
689 doi:10.1029/PA002i006p00561, 1987.

690 Hopkins, T. S.: Recent observations on the intermediate and deep water circulation in the Southern Tyrrhenian
691 Sea, *Oceanol. Acta*, (Special issue), 41–50, 1988.

692 Huang, T. C. and Stanley, D. J.: Western Alboran sea: sediment dispersal, pouncing and reversal of currents, in
693 *The Mediterranean Sea: A Natural Sedimentation Laboratory*, pp. 521–559, Dowden, Hutchinson & Ross,
694 Stroudsburg, PA., 1972.

695 Hutson, W. H.: The Agulhas Current During the Late Pleistocene: Analysis of Modern Faunal Analogs, *Science*
696 (80-.), 207(4426), 64–66, doi:10.1126/science.207.4426.64, 1980.

697 Itambi, a. C., von Dobeneck, T., Mulitza, S., Bickert, T. and Heslop, D.: Millennial-scale northwest African
698 droughts related to Heinrich events and Dansgaard-Oeschger cycles: Evidence in marine sediments from

699 offshore Senegal, *Paleoceanography*, 24(1), PA1205, doi:10.1029/2007PA001570, 2009.

700 Ivy-Ochs, S., Kerschner, H. and Schlüchter, C.: Cosmogenic nuclides and the dating of Lateglacial and Early
701 Holocene glacier variations: The Alpine perspective, *Quat. Int.*, 164-165, 53–63,
702 doi:10.1016/j.quaint.2006.12.008, 2007.

703 Jacobsen, S. B. and Wasserburg, G. J.: Sm-Nd isotopic evolution of chondrites, *Earth Planet. Sci. Lett.*, 50(1),
704 139–155, doi:10.1016/0012-821X(80)90125-9, 1980.

705 Jaffey, A. H., Flynn, K. F., Glendenin, L. E., Bentley, W. C. and Essling, A. M.: Precision measurements of half-
706 lives and specific activities of ²³⁵U and ²³⁸U, *Phys. Rev. C*, 4(5), 1889–1906, doi:10.1103/PhysRevC.4.1889,
707 1971.

708 Jiménez-Espejo, F. J., Pardos-Gené, M., Martínez-Ruiz, F., García-Alix, A., van de Flierdt, T., Toyofuku, T.,
709 Bahr, A. and Kreissig, K.: Geochemical evidence for intermediate water circulation in the westernmost
710 Mediterranean over the last 20kyrBP and its impact on the Mediterranean Outflow, *Glob. Planet. Change*, 135,
711 38–46, doi:10.1016/j.gloplacha.2015.10.001, 2015.

712 Kallel, N., Paterne, M., Labeyrie, L., Duplessy, J.-C. and Arnold, M.: Temperature and salinity records of the
713 Tyrrhenian Sea during the last 18,000 years, *Palaeogeogr. Palaeoclimatol. Palaeoecol.*, 135(1-4), 97–108,
714 doi:10.1016/S0031-0182(97)00021-7, 1997.

715 Kelly, M. A., Ivy-Ochs, S., Kubik, P. W., Von Blanckenburg, F. and Schlüchter, C.: Chronology of deglaciation
716 based on 10 Be dates of glacial erosional features in the Grimsel Pass region, central Swiss Alps, *Boreas*, 35(4),
717 634–643, doi:10.1111/j.1502-3885.2006.tb01169.x, 2006.

718 Khelifi, N., Sarnthein, M., Andersen, N., Blanz, T., Frank, M., Garbe-Schonberg, D., Haley, B. a., Stumpf, R.
719 and Weinelt, M.: A major and long-term Pliocene intensification of the Mediterranean outflow, 3.5-3.3 Ma ago,
720 *Geology*, 37(9), 811–814, doi:10.1130/G30058A.1, 2009.

721 Kinder, T. H. and Parrilla, G.: Yes, some of the Mediterranean water does come from great depth, *J. Geophys.*
722 *Res.*, 92, 2901–2906, doi:10.1029/JC092iC03p02901, 1987.

723 Kuhnt, T., Schmiedl, G., Ehrmann, W., Hamann, Y. and Hemleben, C.: Deep-sea ecosystem variability of the
724 Aegean Sea during the past 22 kyr as revealed by Benthic Foraminifera, *Mar. Micropaleontol.*, 64(3-4), 141–
725 162, doi:10.1016/j.marmicro.2007.04.003, 2007.

726 Kuhnt, T., Schmiedl, G., Ehrmann, W., Hamann, Y. and Andersen, N.: Stable isotopic composition of Holocene
727 benthic foraminifers from the Eastern Mediterranean Sea: Past changes in productivity and deep water
728 oxygenation, *Palaeogeogr. Palaeoclimatol. Palaeoecol.*, 268(1-2), 106–115, doi:10.1016/j.palaeo.2008.07.010,
729 2008.

730 Lacan, F. and Jeandel, C.: Tracing Papua New Guinea imprint on the central Equatorial Pacific Ocean using
731 neodymium isotopic compositions and Rare Earth Element patterns, *Earth Planet. Sci. Lett.*, 186(3-4), 497–512,
732 doi:10.1016/S0012-821X(01)00263-1, 2001.

- 733 Lacan, F. and Jeandel, C.: Neodymium isotopes as a new tool for quantifying exchange fluxes at the continent–
734 ocean interface, *Earth Planet. Sci. Lett.*, 232(3-4), 245–257, doi:10.1016/j.epsl.2005.01.004, 2005.
- 735 Lascaratos, A. and Nittis, K.: A high-resolution three-dimensional numerical study of intermediate water
736 formation in the Levantine Sea, *J. Geophys. Res.*, 103(C9), 18497, doi:10.1029/98JC01196, 1998.
- 737 Lascaratos, A., Williams, R. G. and Tragou, E.: A mixed-layer study of the formation of Levantine intermediate
738 water, *J. Geophys. Res.*, 98(C8), 14739, doi:10.1029/93JC00912, 1993.
- 739 López Correa, M., Montagna, P., Joseph, N., Rüggeberg, A., Fietzke, J., Flögel, S., Dorschel, B., Goldstein, S.
740 L., Wheeler, A. and Freiwald, A.: Preboreal onset of cold-water coral growth beyond the Arctic Circle revealed
741 by coupled radiocarbon and U-series dating and neodymium isotopes, *Quat. Sci. Rev.*, 34, 24–43,
742 doi:10.1016/j.quascirev.2011.12.005, 2012.
- 743 López-Jurado, J. L., Marcos, M. and Monserrat, S.: Hydrographic conditions affecting two fishing grounds of
744 Mallorca island (Western Mediterranean): during the IDEA Project (2003-2004), *J. Mar. Syst.*, 71(3-4), 303–
745 315, doi:10.1016/j.jmarsys.2007.03.007, 2008.
- 746 Ludwig, K. R. and Titterton, D. M.: Calculation of ²³⁰Th/U isochrons, ages, and errors, *Geochim.*
747 *Cosmochim. Acta*, 58(22), 5031–5042, doi:http://dx.doi.org/10.1016/0016-7037(94)90229-1, 1994.
- 748 Lugmair, G. W., Shimamura, T., Lewis, R. S. and Anders, E.: Samarium-146 in the Early Solar System:
749 Evidence from Neodymium in the Allende Meteorite, *Science (80-.)*, 222(4627), 1015–1018,
750 doi:10.1126/science.222.4627.1015, 1983.
- 751 Malanotte-Rizzoli, P., Manca, B. B., D’Alcala, M. R., Theocharis, A., Brenner, S., Budillon, G. and Ozsoy, E.:
752 The Eastern Mediterranean in the 80s and in the 90s: the big transition in the intermediate and deep circulations,
753 *Dyn. Atmos. Ocean.*, 29(2-4), 365–395, doi:10.1016/S0377-0265(99)00011-1, 1999.
- 754 Manca, B., Ibello, V., Pacciaroni, M., Scarazzato, P. and Giorgetti, A.: Ventilation of deep waters in the Adriatic
755 and Ionian Seas following changes in thermohaline circulation of the Eastern Mediterranean, *Clim. Res.*, 31,
756 239–256, doi:10.3354/cr031239, 2006.
- 757 Martrat, B., Grimalt, J. O., Lopez-Martinez, C., Cacho, I., Sierro, F. J., Flores, J. A., Zahn, R., Canals, M.,
758 Curtis, J. H. and Hodell, D. a: Abrupt temperature changes in the Western Mediterranean over the past 250,000
759 years., *Science (80-.)*, 306(5702), 1762–1765, doi:10.1126/science.1101706, 2004.
- 760 Martrat, B., Jimenez-Amat, P., Zahn, R. and Grimalt, J. O.: Similarities and dissimilarities between the last two
761 deglaciations and interglaciations in the North Atlantic region, *Quat. Sci. Rev.*, 99, 122–134,
762 doi:10.1016/j.quascirev.2014.06.016, 2014.
- 763 Melki, T., Kallel, N., Jorissen, F. J., Guichard, F., Dennielou, B., Berné, S., Labeyrie, L. and Fontugne, M.:
764 Abrupt climate change, sea surface salinity and paleoproductivity in the western Mediterranean Sea (Gulf of
765 Lion) during the last 28 kyr, *Palaeogeogr. Palaeoclimatol. Palaeoecol.*, 279(1-2), 96–113,
766 doi:10.1016/j.palaeo.2009.05.005, 2009.

767

768 Mercone, D., Thomson, J., Croudace, I. W., Siani, G., Paterne, M. and Troelstra, S.: Duration of S1, the most
769 recent sapropel in the eastern Mediterranean Sea, as indicated by accelerator mass spectrometry radiocarbon and
770 geochemical evidence, *Paleoceanography*, 15(3), 336–347, doi:10.1029/1999PA000397, 2000.

771 Mercone, D., Thomson, J., Abu-Zied, R. H., Croudace, I. W. and Rohling, E. J.: High-resolution geochemical
772 and micropalaeontological profiling of the most recent eastern Mediterranean sapropel, *Mar. Geol.*, 177(1-2),
773 25–44, doi:10.1016/S0025-3227(01)00122-0, 2001.

774 Millot, C.: Circulation in the Western Mediterranean Sea, *J. Mar. Syst.*, 20(1-4), 423–442, doi:10.1016/S0924-
775 7963(98)00078-5, 1999.

776 Millot, C.: Another description of the Mediterranean Sea outflow, *Prog. Oceanogr.*, 82(2), 101–124,
777 doi:10.1016/j.pocean.2009.04.016, 2009.

778 Millot, C.: Heterogeneities of in- and out-flows in the Mediterranean Sea, *Prog. Oceanogr.*, 120, 254–278,
779 doi:10.1016/j.pocean.2013.09.007, 2014.

780 Millot, C. and Taupier-Letage, I.: Circulation in the Mediterranean Sea, in *Environmental Chemistry*, vol. 5,
781 edited by A. Saliot, pp. 29–66, Springer Berlin Heidelberg, Heidelberg., 2005.

782 Millot, C., Candela, J., Fuda, J.-L. and Tber, Y.: Large warming and salinification of the Mediterranean outflow
783 due to changes in its composition, *Deep Sea Res. Part I Oceanogr. Res. Pap.*, 53(4), 656–666,
784 doi:10.1016/j.dsr.2005.12.017, 2006.

785 Montero-Serrano, J.-C., Frank, N., Colin, C., Wienberg, C. and Eisele, M.: The climate influence on the mid-
786 depth Northeast Atlantic gyres viewed by cold-water corals, *Geophys. Res. Lett.*, 38(19),
787 doi:10.1029/2011GL048733, 2011.

788 Montero-Serrano, J.-C., Frank, N., Tisnérat-Laborde, N., Colin, C., Wu, C., Lin, K., Shen, C., Copard, K.,
789 Orejas, C., Gori, A., De Mol, L., Van Rooij, D., Reverdin, G. and Douville, E.: Decadal changes in the mid-
790 depth water mass dynamic of the Northeastern Atlantic margin (Bay of Biscay), *Earth Planet. Sci. Lett.*, 364,
791 134–144, doi:10.1016/j.epsl.2013.01.012, 2013.

792 Moreno, A., Cacho, I., Canals, M., Prins, M. a., Sánchez-Goñi, M.-F., Grimal, O. J. and Weltje, G. J.: Saharan
793 Dust Transport and High-Latitude Glacial Climatic Variability: The Alboran Sea Record, *Quat. Res.*, 58, 318–
794 328, doi:10.1006/qres.2002.2383, 2002.

795 Moreno, A., Cacho, I., Canals, M., Grimalt, J. O., Sánchez-Goñi, M. F., Shackleton, N. and Sierro, F. J.: Links
796 between marine and atmospheric processes oscillating on a millennial time-scale. A multi-proxy study of the last
797 50,000yr from the Alboran Sea (Western Mediterranean Sea), *Quat. Sci. Rev.*, 24(14-15), 1623–1636,
798 doi:10.1016/j.quascirev.2004.06.018, 2005.

799 Myers, P. G., Haines, K. and Rohling, E. J.: Modeling the paleocirculation of the Mediterranean: The Last
800 Glacial Maximum and the Holocene with emphasis on the formation of sapropel S1, *Paleoceanography*, 13(6),

801 586–606, doi:10.1029/98PA02736, 1998.

802 Ovchinnikov, I. M.: The formation of intermediate water in the Mediterranean, *Oceanology*, 24, 168–173, 1984.

803 Overpeck, J. T., Webb, T. and Prentice, I. C.: Quantitative interpretation of fossil pollen spectra: Dissimilarity
804 coefficients and the method of modern analogs, *Quat. Res.*, 23(1), 87–108, doi:10.1016/0033-5894(85)90074-2,
805 1985.

806 Paterne, M., Kallel, N., Labeyrie, L., Vautravers, M., Duplessy, J.-C., Rossignol-Strick, M., Cortijo, E., Arnold,
807 M. and Fontugne, M.: Hydrological relationship between the North Atlantic Ocean and the Mediterranean Sea
808 during the past 15-75 kyr, *Paleoceanography*, 14(5), 626–638, doi:10.1029/1998PA900022, 1999.

809 Pérez-Folgado, M., Sierro, F. J., Flores, J. A., Cacho, I., Grimalt, J. O., Zahn, R. and Shackleton, N.: Western
810 Mediterranean planktonic foraminifera events and millennial climatic variability during the last 70 kyr, *Mar.
811 Micropaleontol.*, 48(1-2), 49–70, doi:10.1016/S0377-8398(02)00160-3, 2003.

812 Pinardi, N. and Masetti, E.: Variability of the large scale general circulation of the Mediterranean Sea from
813 observations and modelling: a review, *Palaeogeogr. Palaeoclimatol. Palaeoecol.*, 158(3-4), 153–173,
814 doi:10.1016/S0031-0182(00)00048-1, 2000.

815 Piotrowski, A. M., Galy, A., Nicholl, J. a. L., Roberts, N. L., Wilson, D. J., Clegg, J. a. and Yu, J.:
816 Reconstructing deglacial North and South Atlantic deep water sourcing using foraminiferal Nd isotopes, *Earth
817 Planet. Sci. Lett.*, 357-358, 289–297, doi:10.1016/j.epsl.2012.09.036, 2012.

818 Pons-Branchu, E., Douville, E., Roy-Barman, M., Dumont, E., Branchu, P., Thil, F., Frank, N., Bordier, L. and
819 Borst, W.: A geochemical perspective on Parisian urban history based on U–Th dating, laminae counting and
820 yttrium and REE concentrations of recent carbonates in underground aqueducts, *Quat. Geochronol.*, 24, 44–53,
821 doi:10.1016/j.quageo.2014.08.001, 2014.

822 Prell, W. L.: Stability of low-latitude sea-surface temperatures: an evaluation of the CLIMAP reconstruction
823 with emphasis on the positive SST anomalies. Final report, Providence, RI (USA)., 1985.

824 Reimer, P. J., Bard, E., Bayliss, A., Beck, J. W., Blackwell, P. G., Bronk Ramsey, C., Grootes, P. M.,
825 Guilderson, T. P., Hafliðason, H., Hajdas, I., HattĹ, C., Heaton, T. J., Hoffmann, D. L., Hogg, A. G., Hughen, K.
826 A., Kaiser, K. F., Kromer, B., Manning, S. W., Niu, M., Reimer, R. W., Richards, D. A., Scott, E. M., Southon,
827 J. R., Staff, R. A., Turney, C. S. M., & van der Plicht, J. (2013). IntCal13 and Marine13 Radiocarbon Age
828 Calibration Curves 0-50,000 Years cal BP. *Radiocarbon*, 55(4).

829 Revel, M., Colin, C., Bernasconi, S., Combourieu-Nebout, N., Ducassou, E., Grousset, F. E., Rolland, Y.,
830 Migeon, S., Bosch, D., Brunet, P., Zhao, Y. and Mascle, J.: 21,000 Years of Ethiopian African monsoon
831 variability recorded in sediments of the western Nile deep-sea fan, *Reg. Environ. Chang.*, 14(5), 1685–1696,
832 doi:10.1007/s10113-014-0588-x, 2014.

833 Revel, M., Ducassou, E., Skonieczny, C., Colin, C., Bastian, L., Bosch, D., Migeon, S. and Mascle, J.: 20,000
834 years of Nile River dynamics and environmental changes in the Nile catchment area as inferred from Nile upper

- 835 continental slope sediments, *Quat. Sci. Rev.*, 130, 200–221, doi:10.1016/j.quascirev.2015.10.030, 2015.
- 836 Roberts, N. L., Piotrowski, A. M., McManus, J. F. and Keigwin, L. D.: Synchronous deglacial overturning and
837 water mass source changes., *Science*, 327(2010), 75–78, doi:10.1126/science.1178068, 2010.
- 838 Rodrigo-Gámiz, M., Martínez-Ruiz, F., Rampen, S. W., Schouten, S. and Sinninghe Damsté, J. S.: Sea surface
839 temperature variations in the western Mediterranean Sea over the last 20 kyr: A dual-organic proxy (U K' 37 and
840 LDI) approach, *Paleoceanography*, 29(2), 87–98, doi:10.1002/2013PA002466, 2014.
- 841 Rodrigo-Gámiz, M., Martínez-Ruiz, F., Chiaradia, M., Jiménez-Espejo, F. J. and Ariztegui, D.: Radiogenic
842 isotopes for deciphering terrigenous input provenance in the western Mediterranean, *Chem. Geol.*, 410, 237–250,
843 doi:10.1016/j.chemgeo.2015.06.004, 2015.
- 844 Rogerson, M., Rohling, E. J., Weaver, P. P. E. and Murray, J. W.: Glacial to interglacial changes in the settling
845 depth of the Mediterranean Outflow plume, *Paleoceanography*, 20(3), doi:10.1029/2004PA001106, 2005.
- 846 Rogerson, M., Rohling, E. J. and Weaver, P. P. E.: Promotion of meridional overturning by Mediterranean-
847 derived salt during the last deglaciation, *Paleoceanography*, 21(4), 1–8, doi:10.1029/2006PA001306, 2006.
- 848 Rogerson, M., Cacho, I., Jimenez-Espejo, F., Reguera, M. I., Sierro, F. J., Martinez-Ruiz, F., Frigola, J. and
849 Canals, M.: A dynamic explanation for the origin of the western Mediterranean organic-rich layers,
850 *Geochemistry, Geophys. Geosystems*, 9(7), n/a–n/a, doi:10.1029/2007GC001936, 2008.
- 851 Rohling, E. J.: Review and new aspects concerning the formation of eastern Mediterranean sapropels, *Mar.*
852 *Geol.*, 122(1-2), 1–28, doi:10.1016/0025-3227(94)90202-X, 1994.
- 853 Rohling, E. J., Jorissen, F. J. and De stichter, H. C.: 200 Year interruption of Holocene sapropel formation in the
854 Adriatic Sea, *J. Micropalaeontology*, 16(2), 97–108, doi:10.1144/jm.16.2.97, 1997.
- 855 Rohling, E. J., Mayewski, P. a, Abu-Zied, R. H., Casford, J. S. L. and Hayes, A.: Holocene atmosphere-ocean
856 interactions: records from Greenland and the Aegean Sea, *Clim. Dyn.*, 18(7), 587–593, doi:10.1007/s00382-001-
857 0194-8, 2002.
- 858 Rohling, E. J., Sprovieri, M., Cane, T., Casford, J. S. ., Cooke, S., Bouloubassi, I., Emeis, K. C., Schiebel, R.,
859 Rogerson, M., Hayes, A., Jorissen, F. . and Kroon, D.: Reconstructing past planktic foraminiferal habitats using
860 stable isotope data: a case history for Mediterranean sapropel S5, *Mar. Micropaleontol.*, 50(1-2), 89–123,
861 doi:10.1016/S0377-8398(03)00068-9, 2004.
- 862 Rohling, E. J., Marino, G. and Grant, K. M.: Mediterranean climate and oceanography, and the periodic
863 development of anoxic events (sapropels), *Earth-Science Rev.*, 143, 62–97, doi:10.1016/j.earscirev.2015.01.008,
864 2015.
- 865 Rossignol-Strick, M., Nesteroff, W., Olive, P. and Vergnaud-Grazzini, C.: After the deluge: Mediterranean
866 stagnation and sapropel formation, *Nature*, 295(5845), 105–110, doi:10.1038/295105a0, 1982.
- 867 Sammari, C., Millot, C., Taupier-Letage, I., Stefani, A. and Brahim, M.: Hydrological characteristics in the

- 868 Tunisia–Sardinia–Sicily area during spring 1995, *Deep Sea Res. Part I Oceanogr. Res. Pap.*, 46(10), 1671–1703,
869 doi:10.1016/S0967-0637(99)00026-6, 1999.
- 870 Sarmiento, J. L., Herbert, T. and Toggweiler, J. R.: Mediterranean nutrient balance and episodes of anoxia,
871 *Global Biogeochem. Cycles*, 2(4), 427–444, doi:10.1029/GB002i004p00427, 1988.
- 872
- 873 Sánchez-Goñi, M., Cacho, I., Turon, J. L., Guiot, J., Sierro, F. J., Peyrouquet, J., Grimalt, J. O. and Shackleton,
874 N. J.: Synchronicity between marine and terrestrial responses to millennial scale climatic variability during the
875 last glacial period in the Mediterranean region, *Clim. Dyn.*, 19(1), 95–105, doi:10.1007/s00382-001-0212-x,
876 2002.
- 877 Sarnthein, M., Tetzlaff, G., Koopmann, B., Wolter, K. and Pflaumann, U.: Glacial and interglacial wind regimes
878 over the eastern subtropical Atlantic and North-West Africa, *Nature*, 293, 193–196, doi:10.1038/293193a0,
879 1981.
- 880 Scheuven, D., Schütz, L., Kandler, K., Ebert, M. and Weinbruch, S.: Bulk composition of northern African dust
881 and its source sediments — A compilation, *Earth-Science Rev.*, 116, 170–194,
882 doi:10.1016/j.earscirev.2012.08.005, 2013.
- 883 Schmiedl, G., Kuhnt, T., Ehrmann, W., Emeis, K. C., Hamann, Y., Kotthoff, U., Dulski, P. and Pross, J.:
884 Climatic forcing of eastern Mediterranean deep-water formation and benthic ecosystems during the past 22 000
885 years, *Quat. Sci. Rev.*, 29(23-24), 3006–3020, doi:10.1016/j.quascirev.2010.07.002, 2010.
- 886 Schönfeld, J. and Zahn, R.: Late Glacial to Holocene history of the Mediterranean outflow. Evidence from
887 benthic foraminiferal assemblages and stable isotopes at the Portuguese margin, *Palaeogeogr. Palaeoclimatol.*
888 *Palaeoecol.*, 159(1-2), 85–111, doi:10.1016/S0031-0182(00)00035-3, 2000.
- 889 Schott, F., Visbeck, M., Send, U., Fischer, J., Stramma, L. and Desaubies, Y.: Observations of Deep Convection
890 in the Gulf of Lions, Northern Mediterranean, during the Winter of 1991/92, *J. Phys. Oceanogr.*, 26(4), 505–524,
891 doi:10.1175/1520-0485(1996)026<0505:OODCIT>2.0.CO;2, 1996.
- 892 Schroeder, K., Millot, C., Bengara, L., Ben Ismail, S., Bensi, M., Borghini, M., Budillon, G., Cardin, V.,
893 Coppola, L., Curtil, C., Drago, A., El Moumni, B., Font, J., Fuda, J. L., García-Lafuente, J., Gasparini, G. P.,
894 Kontoyiannis, H., Lefevre, D., Puig, P., Raimbault, P., Rougier, G., Salat, J., Sammari, C., Sánchez Garrido, J.
895 C., Sanchez-Roman, A., Sparnocchia, S., Tamburini, C., Taupier-Letage, I., Theocharis, A., Vargas-Yáñez, M.
896 and Vetrano, A.: Long-term monitoring programme of the hydrological variability in the Mediterranean Sea: a
897 first overview of the HYDROCHANGES network, *Ocean Sci.*, 9(2), 301–324, doi:10.5194/os-9-301-2013,
898 2013.
- 899 Scrivner, A. E., Vance, D. and Rohling, E. J.: New neodymium isotope data quantify Nile involvement in
900 Mediterranean anoxic episodes, *Geology*, 32(7), 565, doi:10.1130/G20419.1, 2004.
- 901 Shanahan, T. M., McKay, N. P., Hughen, K. A., Overpeck, J. T., Otto-Bliesner, B., Heil, C. W., King, J., Scholz,
902 C. A. and Peck, J.: The time-transgressive termination of the African Humid Period, *Nat. Geosci.*, 8(2), 140–144,

903 doi:10.1038/ngeo2329, 2015.

904 Siani, G., Paterne, M., Arnold, M., Bard, E., Metivier, B., Tisnerat, N. and Bassinot, F.: Radiocarbon reservoir
905 ages in the Mediterranean Sea and Black Sea, *Radiocarbon*, 42(2), 271–280 [online] Available from: <Go to
906 ISI>://000089971000010, 2000.

907 Siani, G., Paterne, M., Michel, E., Sulpizio, R., Sbrana, A., Arnold, M. and Haddad, G.: Mediterranean Sea
908 surface radiocarbon reservoir age changes since the last glacial maximum., *Science* (80-.), 294(5548), 1917–
909 1920, doi:10.1126/science.1063649, 2001.

910 Siani, G., Sulpizio, R., Paterne, M. and Sbrana, A.: Tephrostratigraphy study for the last 18,000 C years in a
911 deep-sea sediment sequence for the South Adriatic, *Quat. Sci. Rev.*, 23(23-24), 2485–2500,
912 doi:10.1016/j.quascirev.2004.06.004, 2004.

913 Siani, G., Magny, M., Paterne, M., Debret, M., Fontugne, M. (2013) - Paleohydrology reconstruction and
914 Holocene climate variability in the South Adriatic Sea. *Climate of the Past*, 9, 499-515.

915 Sierro, F. J., Hodell, D. A., Curtis, J. H., Flores, J. A., Reguera, I., Colmenero-Hidalgo, E., Bárcena, M. A.,
916 Grimalt, J. O., Cacho, I., Frigola, J. and Canals, M.: Impact of iceberg melting on Mediterranean thermohaline
917 circulation during Heinrich events, *Paleoceanography*, 20(2), n/a–n/a, doi:10.1029/2004PA001051, 2005.

918 Sparnocchia, S., Gasparini, G. P., Astraldi, M., Borghini, M. and Pistek, P.: Dynamics and mixing of the Eastern
919 Mediterranean outflow in the Tyrrhenian basin, *J. Mar. Syst.*, 20(1-4), 301–317, doi:10.1016/S0924-
920 7963(98)00088-8, 1999.

921 Spivack, A. J. and Wasserburg, G. J.: Neodymium isotopic composition of the Mediterranean outflow and the
922 eastern North Atlantic, *Geochim. Cosmochim. Acta*, 52(12), 2767–2773, doi:10.1016/0016-7037(88)90144-5,
923 1988.

924 Stratford, K., Williams, R. G. and Myers, P. G.: Impact of the circulation on Sapropel Formation in the eastern
925 Mediterranean, *Global Biogeochem. Cycles*, 14(2), 683–695, doi:10.1029/1999GB001157, 2000.

926 Stuiver, M., Reimer, P. J. and Reimer, R.: CALIB 7.0, *Radiocarb. Calibration Progr.*, 2005.

927 Tachikawa, K., Roy-Barman, M., Michard, A., Thouron, D., Yeghicheyan, D. and Jeandel, C.: Neodymium
928 isotopes in the Mediterranean Sea: comparison between seawater and sediment signals, *Geochim. Cosmochim.*
929 *Acta*, 68(14), 3095–3106, doi:10.1016/j.gca.2004.01.024, 2004.

930 Tachikawa, K., Piotrowski, A. M. and Bayon, G.: Neodymium associated with foraminiferal carbonate as a
931 recorder of seawater isotopic signatures, *Quat. Sci. Rev.*, 88, 1–13, doi:10.1016/j.quascirev.2013.12.027, 2014.

932 Tanaka, T., Togashi, S., Kamioka, H., Amakawa, H., Kagami, H., Hamamoto, T., Yuhara, M., Orihashi, Y.,
933 Yoneda, S., Shimizu, H., Kunimaru, T., Takahashi, K., Yanagi, T., Nakano, T., Fujimaki, H., Shinjo, R.,
934 Asahara, Y., Tanimizu, M. and Dragusanu, C.: JNdi-1: a neodymium isotopic reference in consistency with
935 LaJolla neodymium, *Chem. Geol.*, 168(3-4), 279–281, doi:10.1016/S0009-2541(00)00198-4, 2000.

- 936 Tachikawa, K., Vidal, L., Cornuault, M., Garcia, M., Pothin, A., Sonzogni, C., Bard, E., Menot, G. and Revel,
937 M.: Eastern Mediterranean Sea circulation inferred from the conditions of S1 sapropel deposition, *Clim. Past*,
938 11(6), 855–867, doi:10.5194/cp-11-855-2015, 2015.
- 939 Taviani, M., Angeletti, L., Canese, S., Cannas, R., Cardone, F., Cau, A., Cau, A. B., Follesa, M. C., Marchese,
940 F., Montagna, P. and Tessarolo, C.: The “Sardinian cold-water coral province” in the context of the
941 Mediterranean coral ecosystems, *Deep Sea Res. Part II Top. Stud. Oceanogr.*, doi:10.1016/j.dsr2.2015.12.008,
942 2015.
- 943 Thunell, R. C. and Williams, D. F.: Glacial–Holocene salinity changes in the Mediterranean Sea: hydrographic
944 and depositional effects, *Nature*, 338(6215), 493–496, doi:10.1038/338493a0, 1989.
- 945 Toucanne, S., Jouet, G., Ducassou, E., Bassetti, M. A., Dennielou, B., Angue Minto’o, C. M., Lahmi, M.,
946 Touyet, N., Charlier, K., Lericolais, G. and Mulder, T.: A 130,000-year record of Levantine Intermediate Water
947 flow variability in the Corsica Trough, western Mediterranean Sea, *Quat. Sci. Rev.*, 33, 55–73,
948 doi:10.1016/j.quascirev.2011.11.020, 2012.
- 949 Vance, D., Scrivner, A. E. and Beney, P.: The use of foraminifera as a record of the past neodymium isotope
950 composition of seawater, *Paleoceanography*, 19(2), PA2009, doi:10.1029/2003PA000957, 2004.
- 951 van de Flierdt, T., Robinson, L. F. and Adkins, J. F.: Deep-sea coral aragonite as a recorder for the neodymium
952 isotopic composition of seawater, *Geochim. Cosmochim. Acta*, 74(21), 6014–6032,
953 doi:10.1016/j.gca.2010.08.001, 2010.
- 954 Voelker, A. H. L., Lebreiro, S. M., Schönfeld, J., Cacho, I., Erlenkeuser, H. and Abrantes, F.: Mediterranean
955 outflow strengthening during northern hemisphere coolings: A salt source for the glacial Atlantic?, *Earth Planet.*
956 *Sci. Lett.*, 245, 39–55, doi:10.1016/j.epsl.2006.03.014, 2006.
- 957 Weaver, A. J., Saenko, O. a., Clark, P. U. and Mitrovica, J. X.: Meltwater Pulse 1A from Antarctica as a Trigger
958 of the Bolling-Allerod Warm Interval, *Science* (80-.), 299(5613), 1709–1713, doi:10.1126/science.1081002,
959 2003.
- 960 Weldeab, S., Emeis, K.-C., Hemleben, C. and Siebel, W.: Provenance of lithogenic surface sediments and
961 pathways of riverine suspended matter in the Eastern Mediterranean Sea: evidence from $^{143}\text{Nd}/^{144}\text{Nd}$ and
962 $^{87}\text{Sr}/^{86}\text{Sr}$ ratios, *Chem. Geol.*, 186(1-2), 139–149, doi:10.1016/S0009-2541(01)00415-6, 2002.
- 963 Weldeab, S., Menke, V. and Schmiedl, G.: The pace of East African monsoon evolution during the Holocene,
964 *Geophys. Res. Lett.*, 41, 1724–1731, doi:10.1002/2014GL059361.Received, 2014.
- 965 Wienberg, C., Frank, N., Mertens, K. N., Stuut, J.-B. W., Marchant, M., Fietzke, J., Mienis, F. and Hebbeln, D.:
966 Glacial cold-water coral growth in the Gulf of Cádiz: Implications of increased palaeo-productivity, *Earth*
967 *Planet. Sci. Lett.*, 298(3-4), 405–416, doi:10.1016/j.epsl.2010.08.017, 2010.
- 968 Wu, Q., Colin, C., Liu, Z., Thil, F., Dubois-Dauphin, Q., Frank, N., Tachikawa, K., Bordier, L. and Douville, E.:
969 Neodymium isotopic composition in foraminifera and authigenic phases of the South China Sea sediments:

970 Implications for the hydrology of the North Pacific Ocean over the past 25 kyr, *Geochemistry, Geophys.*
971 *Geosystems*, 16(11), 3883–3904, doi:10.1002/2015GC005871, 2015.

972 **Table captions**

973

974 **Table 1.** U-series ages and ϵNd values obtained for cold-water coral samples collected from sediment core RECORD 23
975 (Sardinia Channel).

976

977 **Table 2.** ϵNd values obtained for cold-water corals from the southern Alboran Sea. The AMS ^{14}C ages published by Fink et
978 al. (2013) are also reported as Median probability age (ka BP).

979

980 **Table 3.** AMS ^{14}C ages of samples of the planktonic foraminifer *G. bulloides* from ‘off-mound’ sediment core SU92-33. The
981 AMS ^{14}C ages were corrected for ^{13}C and a mean reservoir age of 400 yrs, and were converted into calendar years using the
982 INTCAL13 calibration data set (Reimer et al., 2013) and the CALIB 7.0 program (Struiver et al., 2005).

983

984 **Table 4.** Multiproxy data obtained for the upper 2.1 m of sediment core SU92-33 (Balearic Sea). Stable oxygen and carbon
985 isotopes were measured on benthic (*C. pachyderma*) and planktonic (*G. bulloides*) foraminifera; ϵNd values were obtained on
986 mixed planktonic foraminifera samples. The age results from a combination of 7 AMS- ^{14}C age measurements for the upper
987 1.2 m of the core and by a linear interpolation between these ages as well as the $\delta^{18}\text{O}$ variations of the planktonic
988 foraminifera *G. bulloides*.

989

990 **Figure captions**

991

992 **Figure 1.** Map of the western Mediterranean Sea showing the locations of samples investigated in this study. Yellow dot
993 indicates the sampling location of the sediment core from the Balearic Sea (SU92-33); yellow stars indicate the locations of
994 the CWC-bearing cores from the Sardinia Channel (RECORD 23) and the southern Alboran Sea (for further details on the
995 CWC from the Alboran Sea refer also to Fink et al., 2013). The cores discussed in this paper (Gulf of Cádiz: IODP site
996 U1387, Balearic Sea: MD09-2343, northern Tyrrhenian Sea: MD01-2472, Adriatic Sea: MD90-917) are indicated by black
997 dots, and seawater stations are marked by open squares. Arrows represent the main oceanographic currents. The black line
998 shows the general trajectory of the Modified Atlantic Water (MAW) flowing at the surface from the Atlantic Ocean toward
999 the western and eastern Mediterranean. The orange line represents the Levantine Intermediate Water (LIW) originating from
1000 the eastern basin. The black dashed line shows the trajectory of the Western Mediterranean Deep Water (WMDW) flowing
1001 from the Gulf of Lions toward the Strait of Gibraltar.

1002

1003 **Figure 2.** (a) Sea Surface Temperature (SST) records of cores SU92-33 (red line) and MD90-917 (green line; Siani et al.,
1004 2004), (b) $\delta^{18}\text{O}$ record obtained on planktonic foraminifer *G. bulloides* for core SU92-33, (c) $\delta^{18}\text{O}$ record obtained on benthic
1005 foraminifer *C. pachyderma* for core SU92-33, (d) $\delta^{13}\text{C}$ record obtained on benthic foraminifer *C. pachyderma* for core SU92-
1006 33. LGM: Last Glacial Maximum; HS1: Heinrich Stadial 1; B-A: Bølling-Allerød; YD: Younger Dryas. Black triangles
1007 indicate AMS ^{14}C age control points.

1008

1009 **Figure 3.** (a) Sea Surface Temperature (SST) record of core SU92-33 (red line), (b) ϵNd records obtained on mixed
1010 planktonic foraminifers from core SU92-33 (open circles) and from cold-water coral fragments collected in the Alboran Sea
1011 (red squares), (c) ϵNd values of cold-water corals from core RECORD 23 (Sardinia Channel).

1012

1013 **Figure 4.** (a) $\delta^{13}\text{C}$ records obtained on benthic foraminifer *C. pachyderma* for cores SU92-33 (red line) and MD99-2343
1014 (blue line; Sierro et al., 2005). (b) ϵNd records obtained on mixed planktonic foraminifers from core SU92-33 (open circles)
1015 and from cold-water coral fragments collected in the Alboran Sea (red squares). Modern ϵNd values for LIW (orange dashed
1016 line) and WMDW (blue dashed line) are also reported for comparison. (c) ϵNd values obtained for planktonic foraminifera
1017 with Fe-Mn coatings at sites 300G (36°21.532' N, 1°47.507' W; 1860 m; open dots) and 304G (36°19.873' N, 1°31.631' W;
1018 2382 m; black dots) in Alboran Sea (Jimenez-Espejo et al., 2015). (d) UP10 fraction (>10 μm) from core MD99-2343
1019 (Frigola et al., 2008). (e) Sortable silt mean grain-size of core MD01-2472 (Toucanne et al., 2012). (f) Ln Zr/Al ratio at IODP
1020 site U1387 (36°48.3' N 7°43.1' W; 559 m) (Bahr et al., 2015).

1021
1022 **Figure 5.** (a) $\delta^{18}\text{O}$ record obtained on planktonic foraminifer *G. bulloides* for core SU92-33, (b) $\delta^{13}\text{C}$ records obtained on
1023 benthic foraminifer *C. pachyderma* for core SU92-33, (c) ϵNd values of cold-water corals from core RECORD 23 (Sardinia
1024 Channel), (d) ϵNd values records obtained on mixed planktonic foraminifera from core SU92-33 (open circles) and from
1025 cold-water coral fragments collected in the Alboran Sea (red squares), (e) ϵNd values obtained on terrigenous fraction of
1026 MS27PT located close the Nile River mouth in the eastern Mediterranean basin (Revel et al., 2015)

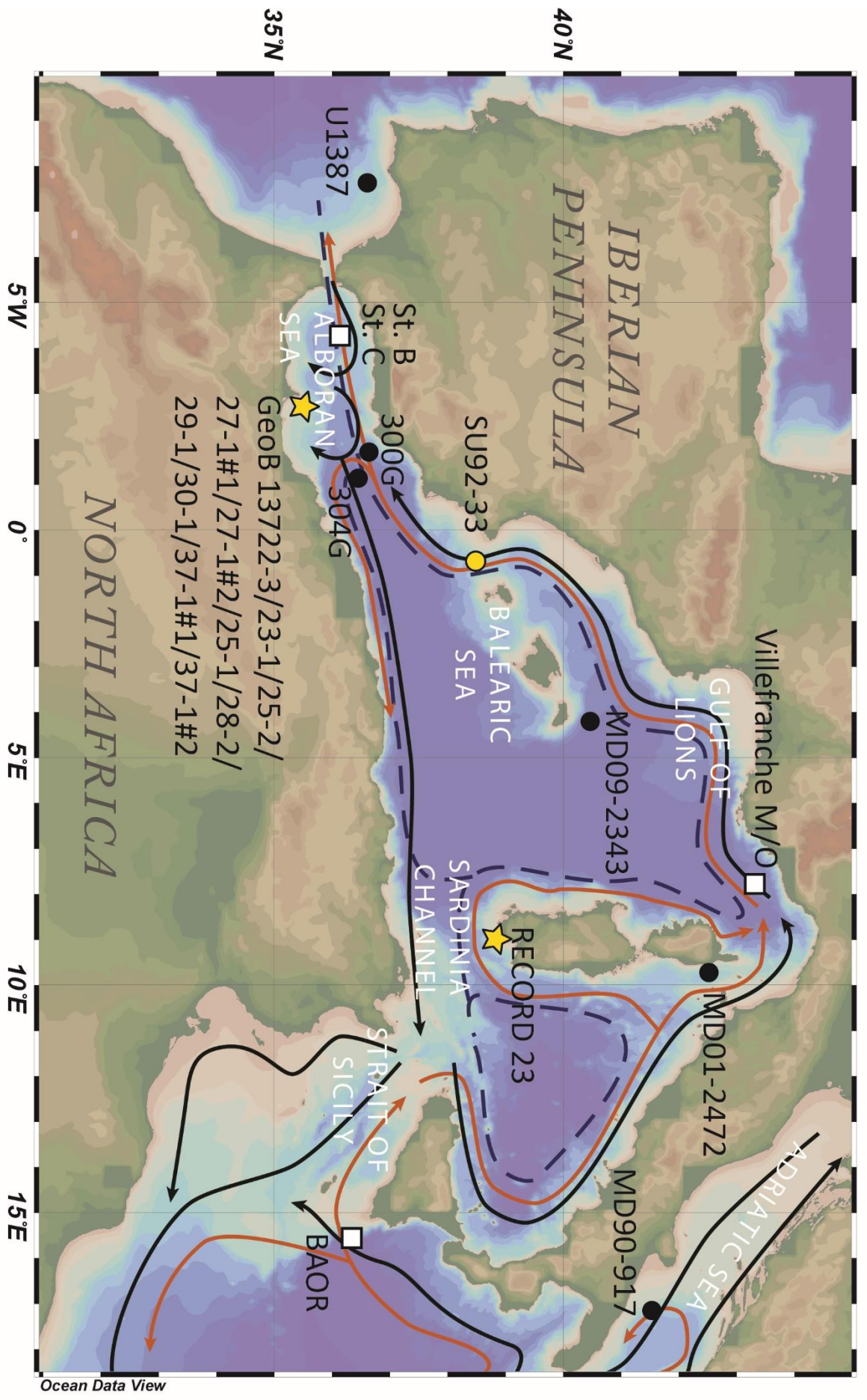


Figure 1

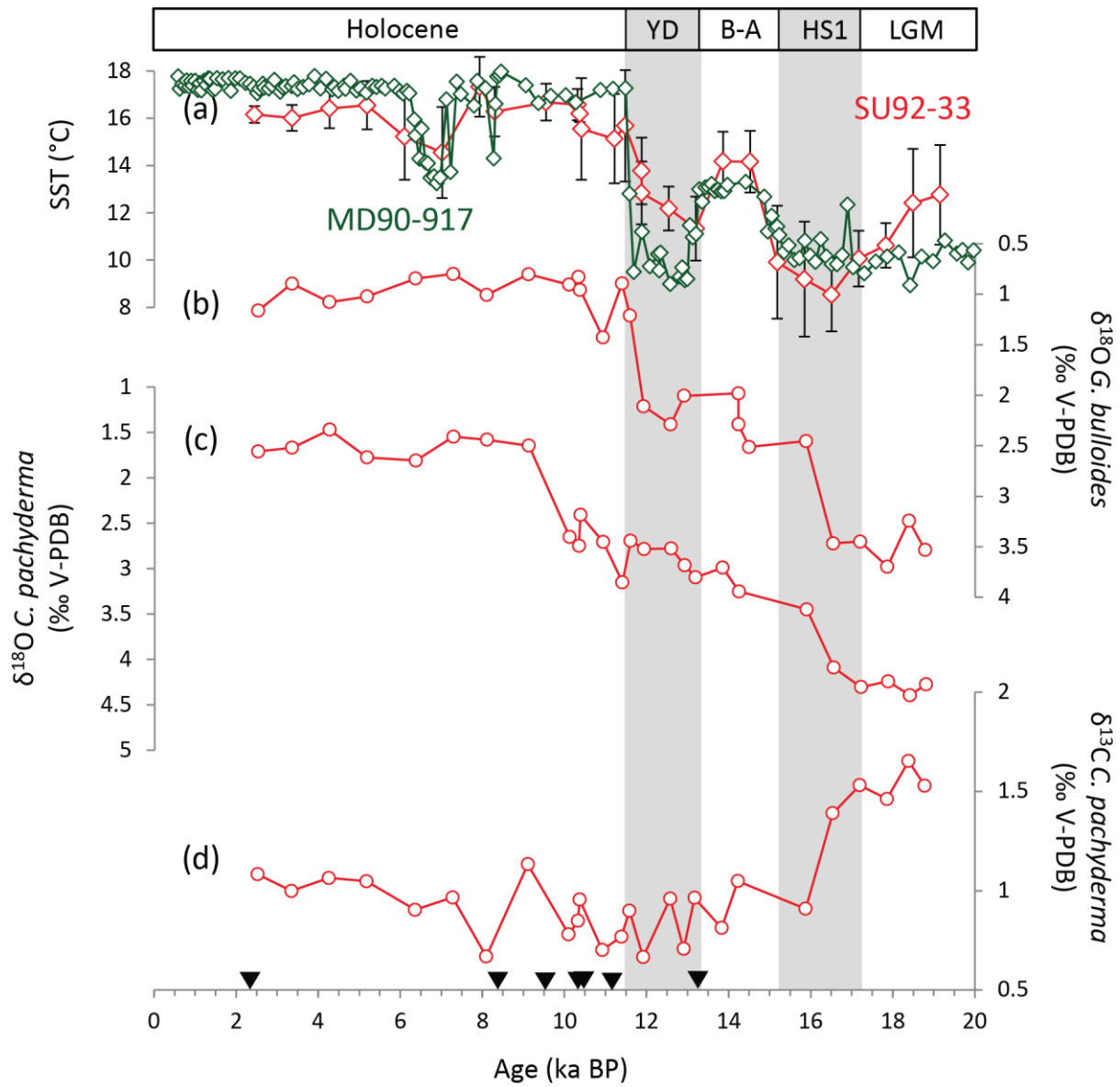


Figure 2

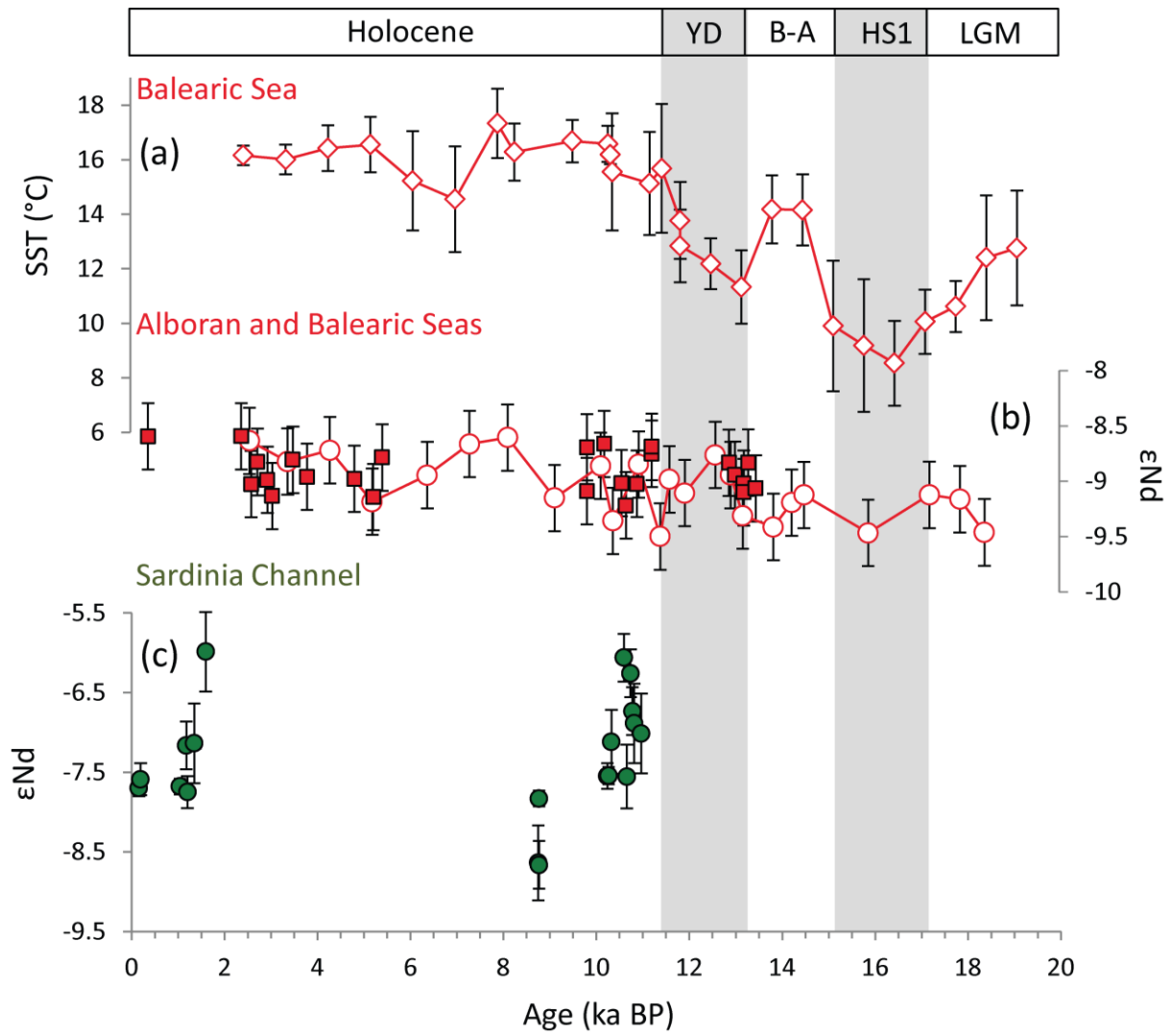


Figure 3

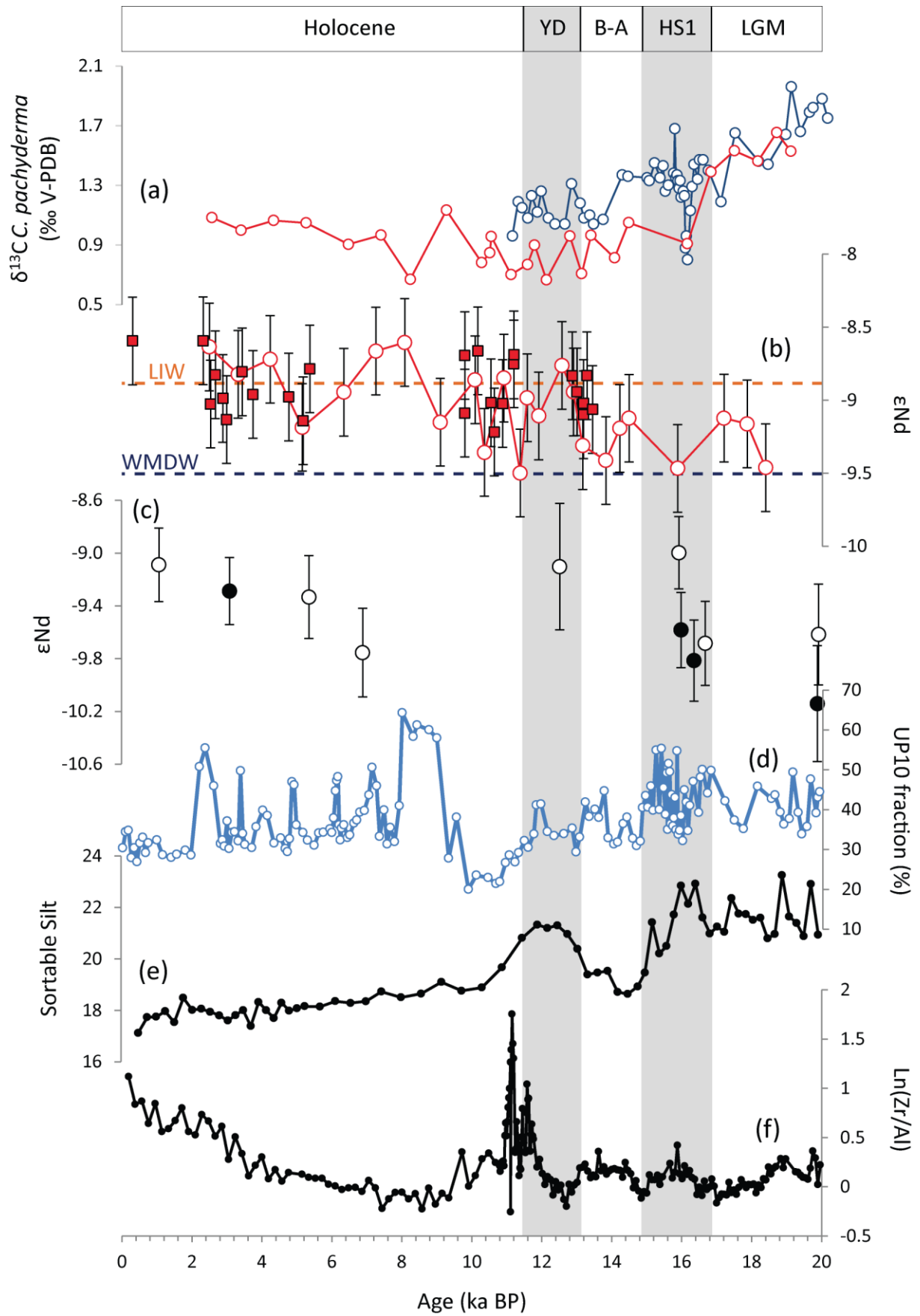


Figure 4

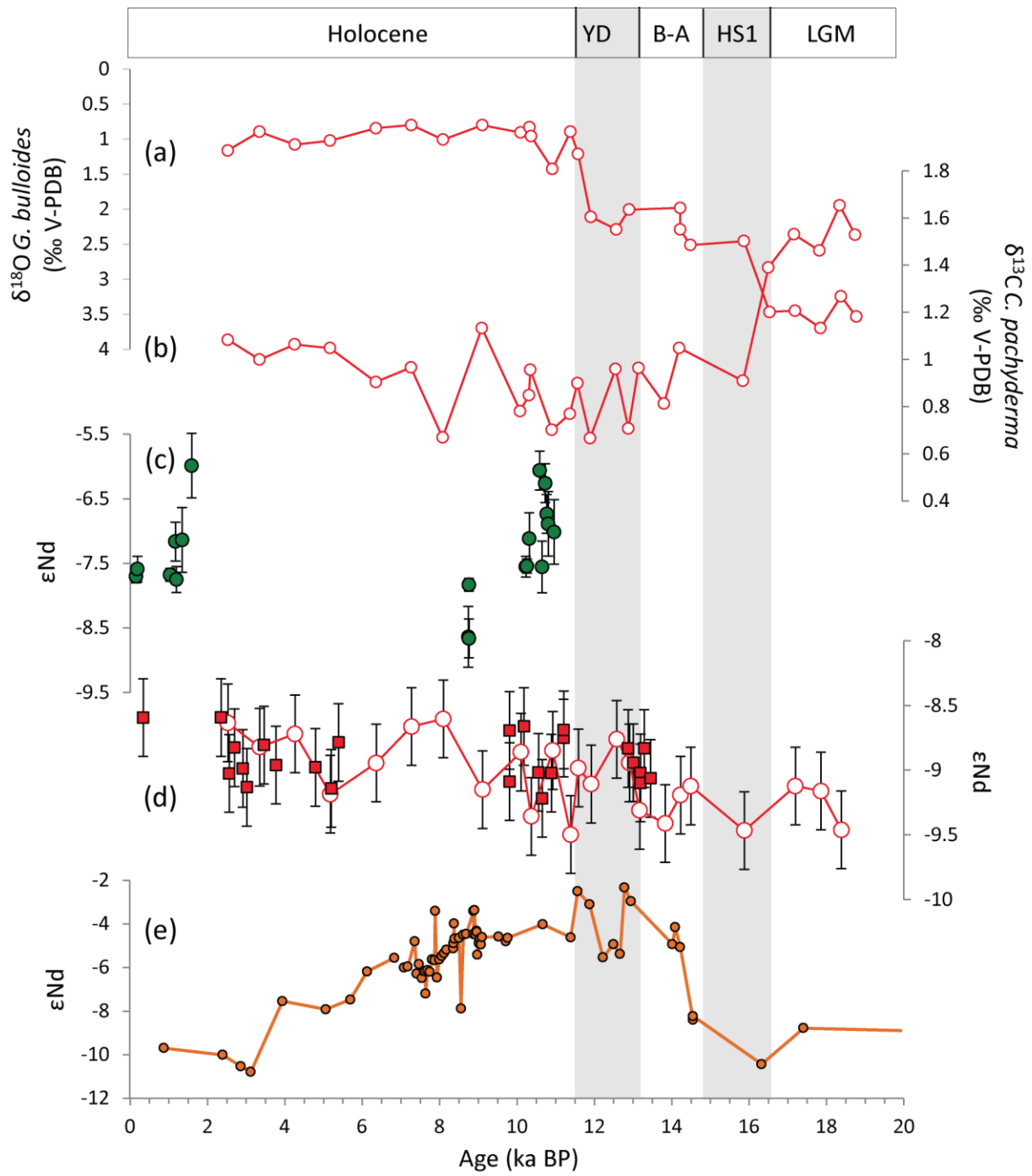


Figure 5

Sample ID	Depth in core (cm)	Corals species	^{238}U ($\mu\text{g/g}$)	^{232}Th (ng/g)	$\delta^{234}\text{U}_m$ (‰)	$^{230}\text{Th}/^{238}\text{U}$	$^{230}\text{Th}/^{232}\text{Th}$	Age (ka BP)	$\delta^{234}\text{U}_{(t)}$ (‰)	$^{143}\text{Nd}/^{144}\text{Nd}$	ϵNd
RECORD_23_V	0-3,5	<i>Madrepora oculata</i>	3.31 \pm 0.005	0.68 \pm 0.014	151.85 \pm 1.7	0.00163 \pm 0.00011	25 \pm 1.7	0.091 \pm 0.011	151.92 \pm 1.7	0.512243 \pm 0.000005	-7.70 \pm 0.10
RECORD_23_V	3-7	<i>Madrepora oculata</i>	3.23 \pm 0.002	0.52 \pm 0.001	147.11 \pm 0.6	0.00199 \pm 0.00006	38 \pm 1.1	0.127 \pm 0.006	147.19 \pm 0.6	0.512249 \pm 0.000010	-7.59 \pm 0.20
RECORD_23_V	7-10	<i>Madrepora oculata</i>	3.99 \pm 0.007	0.25 \pm 0.002	147.52 \pm 1.7	0.01227 \pm 0.00022	640 \pm 11.6	1.110 \pm 0.023	148.01 \pm 1.7	0.512244 \pm 0.000015	-7.68 \pm 0.30
RECORD_23_V	8-10	<i>Madrepora oculata</i>	3.79 \pm 0.005	0.41 \pm 0.001	148.47 \pm 0.7	0.01253 \pm 0.00007	350 \pm 2.0	1.135 \pm 0.008	148.27 \pm 0.7	0.512271 \pm 0.000010	-7.16 \pm 0.20
RECORD_23_IV	6-9	<i>Madrepora oculata</i>	4.06 \pm 0.006	0.35 \pm 0.001	148.47 \pm 1.3	0.01366 \pm 0.00011	480 \pm 3.8	1.243 \pm 0.012	149.02 \pm 1.2	0.512241 \pm 0.000010	-7.75 \pm 0.20
RECORD_23_IV	27-30	<i>Madrepora oculata</i>	4.06 \pm 0.003	1.09 \pm 0.001	146.91 \pm 1.3	0.01405 \pm 0.00013	159 \pm 1.4	1.283 \pm 0.014	147.47 \pm 1.3	0.512272 \pm 0.000026	-7.14 \pm 0.50
RECORD_23_IV	37-40	<i>Madrepora oculata</i>	3.52 \pm 0.005	0.08 \pm 0.000	148.25 \pm 1.1	0.01663 \pm 0.00012	2308 \pm 16.4	1.529 \pm 0.013	148.92 \pm 1.1	0.512331 \pm 0.000026	-5.99 \pm 0.50
RECORD_23_III	55-57	<i>Madrepora oculata</i>	3.63 \pm 0.002	0.27 \pm 0.000	145.30 \pm 0.7	0.08859 \pm 0.00020	3530 \pm 8.1	8.685 \pm 0.027	148.93 \pm 0.8	0.512195 \pm 0.000026	-8.64 \pm 0.50
RECORD_23_III	58-61	<i>Madrepora oculata</i>	4.24 \pm 0.004	0.36 \pm 0.001	146.71 \pm 1.2	0.08863 \pm 0.00037	3336 \pm 14.0	8.702 \pm 0.048	150.39 \pm 1.2	0.512237 \pm 0.000010	-7.83 \pm 0.20
RECORD_23_III	63-66	<i>Lophelia pertusa</i>	4.15 \pm 0.005	0.42 \pm 0.002	147.19 \pm 0.8	0.08863 \pm 0.00054	2783 \pm 17.1	8.703 \pm 0.063	150.89 \pm 0.9	0.512194 \pm 0.000015	-8.66 \pm 0.30
RECORD_23_I	0-2	<i>Lophelia pertusa</i>	3.35 \pm 0.002	0.37 \pm 0.000	147.02 \pm 0.7	0.10283 \pm 0.00018	2788 \pm 4.8	10.173 \pm 0.025	151.34 \pm 0.7	0.512251 \pm 0.000010	-7.55 \pm 0.20
RECORD_23_II	62-65	<i>Lophelia pertusa</i>	3.27 \pm 0.003	0.39 \pm 0.002	144.75 \pm 1.2	0.10289 \pm 0.00061	2721 \pm 16.1	10.201 \pm 0.075	149.01 \pm 1.2	0.512251 \pm 0.000010	-7.54 \pm 0.20
RECORD_23_II	50-52	<i>Lophelia pertusa</i>	2.92 \pm 0.003	0.92 \pm 0.003	145.39 \pm 1.6	0.10351 \pm 0.00061	1046 \pm 6.2	10.260 \pm 0.079	149.69 \pm 1.6	0.512273 \pm 0.000021	-7.12 \pm 0.40
RECORD_23_I	12-14	<i>Lophelia pertusa</i>	3.07 \pm 0.002	0.49 \pm 0.000	145.22 \pm 0.7	0.10609 \pm 0.00023	1971 \pm 4.3	10.531 \pm 0.031	149.64 \pm 0.7	0.512327 \pm 0.000015	-6.06 \pm 0.30
RECORD_23_I	5-7	<i>Lophelia pertusa</i>	3.50 \pm 0.002	0.42 \pm 0.000	146.35 \pm 0.9	0.10677 \pm 0.00016	2654 \pm 4.0	10.591 \pm 0.025	150.82 \pm 0.9	0.512251 \pm 0.000021	-7.55 \pm 0.40
RECORD_23_II	94-98	<i>Lophelia pertusa</i>	3.14 \pm 0.003	0.62 \pm 0.002	146.42 \pm 1.0	0.10755 \pm 0.00047	1737 \pm 7.6	10.672 \pm 0.059	150.94 \pm 1.0	0.512317 \pm 0.000015	-6.26 \pm 0.30
RECORD_23_I	15-17	<i>Lophelia pertusa</i>	3.40 \pm 0.003	0.46 \pm 0.000	146.01 \pm 0.9	0.10790 \pm 0.00021	2409 \pm 4.6	10.713 \pm 0.031	150.53 \pm 0.9	0.512293 \pm 0.000015	-6.73 \pm 0.30
RECORD_23_II	96-100	<i>Lophelia pertusa</i>	3.61 \pm 0.004	0.35 \pm 0.001	145.50 \pm 0.8	0.10821 \pm 0.00044	3579 \pm 14.7	10.750 \pm 0.055	150.02 \pm 0.8	0.512285 \pm 0.000026	-6.89 \pm 0.50
RECORD_23_II	93-95	<i>Lophelia pertusa</i>	3.19 \pm 0.003	0.24 \pm 0.000	143.33 \pm 0.8	0.10947 \pm 0.00032	4381 \pm 12.7	10.904 \pm 0.042	147.85 \pm 0.9	0.512279 \pm 0.000026	-7.01 \pm 0.50

Table 1

Sample ID	Core depth (cm)	Species	Water Depth (m)	Median probability age (ka BP)	$^{143}\text{Nd}/^{144}\text{Nd}$	ϵNd
GeoB 13727-1#1	Surface	<i>Lophelia pertusa</i>	363	0.339	0.512198 ±0.000015	-8.59 ±0.30
GeoB 13727-1#2	Surface	<i>Madrepora oculata</i>	353	2.351	0.512198 ±0.000015	-8.59 ±0.30
GeoB 13730-1	6	<i>Lophelia pertusa</i>	338	2.563	0.512175 ±0.000015	-9.03 ±0.30
GeoB 13728-1	Bulk (0-15)	<i>Lophelia pertusa</i>	343	2.698	0.512185 ±0.000015	-8.83 ±0.30
GeoB 13728-2	2	<i>Lophelia pertusa</i>	343	2.913	0.512177 ±0.000015	-8.99 ±0.30
GeoB 13722-3	Bulk (0-15)	<i>Madrepora oculata</i>	280	3.018	0.512170 ±0.000015	-9.13 ±0.30
GeoB 13722-3	Bulk (15-30)	<i>Madrepora oculata</i>	280	3.463	0.512186 ±0.000015	-8.81 ±0.30
GeoB 13735-1	Bulk (0-15)	<i>Madrepora oculata</i>	280	3.770	0.512179 ±0.000015	-8.96 ±0.30
GeoB 13723-1	Bulk (0-8)	<i>Madrepora oculata</i>	291	4.790	0.512178 ±0.000015	-8.98 ±0.30
GeoB 13725-2	Surface	<i>Madrepora oculata</i>	355	5.201	0.512169 ±0.000015	-9.14 ±0.30
GeoB 13723-1	Bulk (8-20)	<i>Madrepora oculata</i>	291	5.390	0.512187 ±0.000015	-8.79 ±0.30
GeoB 13729-1	2.5	<i>Lophelia pertusa</i>	442	9.810	0.512172 ±0.000015	-9.09 ±0.30
GeoB 13729-1	2.5	<i>Lophelia pertusa</i>	442	9.810	0.512193 ±0.000015	-8.69 ±0.30
GeoB 13729-1	49	<i>Lophelia pertusa</i>	442	10.181	0.512194 ±0.000015	-8.66 ±0.30
GeoB 13730-1	102	<i>Lophelia pertusa</i>	338	10.556	0.512176 ±0.000015	-9.02 ±0.30
GeoB 13730-1	194	<i>Lophelia pertusa</i>	338	10.652	0.512165 ±0.000015	-9.22 ±0.30
GeoB 13729-1	315	<i>Lophelia pertusa</i>	442	10.889	0.512176 ±0.000015	-9.02 ±0.30
GeoB 13729-1	375	<i>Lophelia pertusa</i>	442	11.206	0.512189 ±0.000015	-8.75 ±0.30
GeoB 13730-1	298	<i>Lophelia pertusa</i>	338	11.208	0.512193 ±0.000015	-8.69 ±0.30
GeoB 13728-2	191	<i>Lophelia pertusa</i>	343	12.874	0.512185 ±0.000015	-8.83 ±0.30
GeoB 13737-1#2	Surface	<i>Lophelia pertusa</i>	297	13.005	0.512180 ±0.000015	-8.94 ±0.30
GeoB 13728-2	295	<i>Lophelia pertusa</i>	364	13.194	0.512176 ±0.000015	-9.02 ±0.30
GeoB 13728-2	295	<i>Lophelia pertusa</i>	364	13.194	0.512171 ±0.000015	-9.10 ±0.30
GeoB 13730-1	427	<i>Lophelia pertusa</i>	338	13.291	0.512185 ±0.000015	-8.83 ±0.30
GeoB 13737-1#1	Surface	<i>Lophelia pertusa</i>	299	13.452	0.512174 ±0.000015	-9.06 ±0.30

Table 2

Core	Depth in core (cm)	¹⁴ C-age (years)	±1σ (years)	Median probability age (ka BP)
SU92-33	0	2770	70	2437
SU92-33	64	7870	90	8280
SU92-33	70	8670	80	9528
SU92-33	74	9510	100	10295
SU92-33	84	9610	90	10389
SU92-33	90	10180	100	11192
SU92-33	120	11710	110	13172

Table 3

Depth in core (cm)	Age (ka BP)	$\delta^{13}\text{C}$		$\delta^{18}\text{O}$		$^{143}\text{Nd}/^{144}\text{Nd}$	ϵNd
		<i>C. pachyderma</i> (‰ VPDB)	<i>C. pachyderma</i> (‰ VPDB)	<i>G. bulloides</i> (‰ VPDB)	<i>G. bulloides</i> (‰ VPDB)		
1	2.53	1.08	1.71	-0.6	1.16	0.512195 ±0.000015	-8.64 ±0.30
10	3.35	1.00	1.67	-0.82	0.90	0.512186 ±0.000015	-8.82 ±0.30
19.5	4.26	1.06	1.47	-0.55	1.08	0.512191 ±0.000015	-8.72 ±0.30
29.5	5.18	1.05	1.78	-0.55	1.02	0.512167 ±0.000015	-9.19 ±0.30
42.5	6.36	0.90	1.81	-0.91	0.84	0.512179 ±0.000015	-8.95 ±0.30
52.5	7.28	0.97	1.55	-0.80	0.80	0.512194 ±0.000015	-8.66 ±0.30
61.5	8.10	0.67	1.58	-0.95	1.01	0.512197 ±0.000015	-8.61 ±0.30
67.5	9.11	1.13	1.65	-1.07	0.80	0.512169 ±0.000015	-9.15 ±0.30
72.5	10.10	0.78	2.65	-1.27	0.91	0.512184 ±0.000015	-8.86 ±0.30
77.5	10.33	0.85	2.75	-1.10	0.83	-	-
81.5	10.37	0.96	2.41	-1.21	0.96	0.512158 ±0.000015	-9.36 ±0.30
87.5	10.92	0.70	2.71	-0.11	1.43	0.512184 ±0.000015	-8.85 ±0.30
92.5	11.39	0.77	3.15	-1.00	0.89	0.512151 ±0.000015	-9.50 ±0.30
95.5	11.59	0.90	2.69	-1.14	1.21	0.512178 ±0.000015	-8.98 ±0.30
100.5	11.92	0.67	2.78	-0.44	2.11	0.512171 ±0.000015	-9.11 ±0.30
110.5	12.58	0.96	2.78	-0.86	2.29	0.512189 ±0.000015	-8.76 ±0.30
115.5	12.91	0.71	2.96	-0.54	2.01	0.512180 ±0.000015	-8.94 ±0.30
119.5	13.17	0.96	3.09	-	-	0.512161 ±0.000015	-9.31 ±0.30
129.5	13.83	0.81	2.99	-	-	0.512156 ±0.000015	-9.41 ±0.30
135.5	14.23	1.05	3.25	-1.16	1.98	0.512167 ±0.000015	-9.19 ±0.30
135.5	14.23	-	-	-0.94	2.29	-	-
139.5	14.49	-	-	-0.96	2.51	0.512170 ±0.000015	-9.12 ±0.30
159.5	15.88	0.91	3.45	-0.81	2.45	0.512153 ±0.000015	-9.47 ±0.30
169.5	16.54	1.39	4.09	-0.76	3.47	-	-
179.5	17.20	1.53	4.30	-0.98	3.45	0.512170 ±0.000015	-9.12 ±0.30
190	17.86	1.46	4.24	-1.10	3.70	0.512168 ±0.000015	-9.16 ±0.30
198	18.39	1.65	4.39	-1.24	3.24	0.512153 ±0.000015	-9.46 ±0.30
206	18.78	1.53	4.28	-0.90	3.53	-	-

Table 4